Beta-Glucan Modulates Monocyte Plasticity and Differentiation Capacity to Mitigate DSS-Induced Colitis

Yinyin Lv[#1,3,4], Yanyun Fan[#1,3,4], Qingxiang Gao[#2], Qiongyun Chen[#3,4,6], Yiqun Hu[1,3,4], Lin Wang[1,3,4], Huaxiu Shi[1,3,4], Ermei Chen[1,3,4], Qinyu Xu[1,3,4], Ying Cai[1,3,4], Qingqi Fan[2], Linying Li[2], Dan Du[5], Jianlin Ren[1,3,4*], Shih-Chin Cheng [2,4*], Hongzhi Xu[1,3,4*]

[1]Department of Gastroenterology, The National Key Clinical Specialty, Zhongshan Hospital of Xiamen University, School of Medicine, Xiamen University, Xiamen 361004, Fujian Province, P.R. China

[2]State Key Laboratory of Cellular Stress Biology, School of Life Sciences, Faculty of Medicine and Life Sciences, Xiamen University, Xiamen, Fujian 361102, China

[3]Clinical Research Center for Gut Microbiota and Digestive Diseases of Fujian Province, Xiamen Key Laboratory of Intestinal Microbiome and Human Health，Xiamen 361004, Fujian Province, P. R. China

[4]Department of Digestive Disease, Institute for Microbial Ecology, School of Medicine, Xiamen University, Xiamen 361004, Fujian Province, P. R. China

[5]State Key Laboratory of Cellular Stress Biology, Department of Gastroenterology, Zhongshan Hospital of Xiamen University, School of Medicine, Faculty of Medicine and Life Sciences, Xiamen University, Xiamen 361102, China

[6]Department of Gastroenterology, Taikang Xianlin Drum Tower Hospital, Affiliated Hospital of Medical School, Nanjing University, Nanjing, China

Author contributions: [#]These authors contributed equally work.

[*]**Corresponding author:**

HongzhiXu (E-mail: xuhongzhi@xmu.edu.cn)

Shih-ChinCheng (E-mail: jamescheng@xmu.edu.cn)

Jianlin Ren (E-mail: jianlin.ren@126.com)

Declaration of interests: The authors declare no competing interests.

Abstract:

Trained immunity involves the reprogramming of innate immune cells after an initial exposure, resulting in heightened inflammatory responses to subsequent stimuli and enhanced bactericidal capacity during infection. However, this proinflammatory state could also exacerbate chronic conditions like inflammatory bowel disease (IBD), which is characterized by persistent inflammation and microbial imbalance. It remains unclear how trained immunity influences IBD pathogenesis and whether it can be harnessed therapeutically. In our study, pretreatment with β-glucan reprogrammed bone marrow hematopoietic progenitors and peripheral monocytes, inducing a profound shift in monocyte plasticity and significantly reducing the severity of dextran sulfate sodium (DSS)–induced colitis. Adoptive transfer of bone marrow or peripheral monocytes from β-glucan–trained mice into naive mice conferred robust protection against colitis, demonstrating that this protective effect is transferable. Trained mice also displayed improved clearance of intestinal bacterial infections. Single-cell RNA sequencing revealed an expansion of reparative $Cx3cr1^{+}$ macrophages derived from $Ly6C^{hi}$ monocytes, correlating with accelerated colonic epithelial regeneration. Collectively, these findings reveal how β-glucan–induced trained immunity modulates monocyte differentiation to ameliorate experimental colitis, highlighting the potential of harnessing trained immunity as a therapeutic strategy to recalibrate innate immune responses and restore gut homeostasis in IBD, shedding light for future clinical applications.

Keywords: Trained immunity, Monocyte/Macrophage, Colitis

Introduction

Inflammatory bowel disease (IBD), encompassing ulcerative colitis (UC) and Crohn's disease (CD), is a chronic gastrointestinal inflammatory disorder associated with significant morbidity(1, 2). The intestinal mucosa is continuously exposed to a diverse microbial ecosystem, including fungi, bacteria, and viruses(3). In IBD, the delicate balance between the immune system and the microbiota is disrupted, leading to uncontrolled inflammation(4, 5). This dysregulation is further exacerbated by genetic factors, such as loss-of-function mutations in NOD2, which impair antimicrobial peptide production, increase susceptibility to intestinal infections, and decrease IL-10 production by monocytes(6-8).

Trained immunity, a phenomenon where innate immune cells exhibit enhanced responses to secondary challenges, has emerged as a promising therapeutic avenue for various infectious diseases and cancer(9-13). However, its role in chronic inflammatory conditions like IBD remains largely unexplored. While trained immunity can enhance pathogen clearance, it also involves the upregulation of pro-inflammatory cytokines such as TNF, IL-1β, and IL-6(14), therefore the role of trained immunity in IBD remained elusive.

This study aimed to investigate the therapeutic potential of trained immunity in a mouse model of colitis. We hypothesized that inducing trained immunity could enhance microbial control, thereby preserving intestinal integrity and ultimately mitigating disease severity. To test this, we employed β-glucan (BG), a prototypic trained immunity inducer, and assessed its impact on dextran sulfate sodium (DSS)-induced colitis. Our findings demonstrate that BG pretreatment significantly alleviates colitis in mice. Mechanistically, BG induced central immunity in the hematopoietic compartment, leading to the generation of "trained" monocytes in the periphery. Both bone marrow transplantation from trained donors and adoptive transfer of trained monocytes conferred protection against DSS-induced colitis. Furthermore, single-cell RNA-seq revealed that BG-induced trained immunity promotes the expansion of reparative Cx3cr1 intestinal macrophages derived from Ly6C^{hi} monocytes, thereby facilitating epithelial regeneration. In summary, our data suggest that harnessing trained immunity represents a promising therapeutic approach for IBD treatment.

Results

β-glucan (BG) pretreatment ameliorates DSS-induced colitis

To investigate the impact of trained immunity on colitis, mice were pretreated with BG, a potent inducer of trained immunity. Successful induction of BG-induced trained immunity (BGTI) was confirmed by the enhanced resistance to *Staphylococcus aureus* infection in BG-treated mice (**Fig S1A and S1B**), consistent with previous findings(15). Importantly, BG-pretreatment did not induce spontaneous intestinal inflammation (**Fig S1C and S1D)**. Following BGTI induction, mice were subjected to DSS-induced colitis. (**Fig 1A**). BG pretreatment significantly ameliorated disease severity, as indicated by the reduced body weight loss (**Fig 1B and Fig S1E**), colon shortening (**Fig 1C and Fig S1F and S1G**), and diminished mucosal inflammation observed via endoscopic imaging (**Fig 1D**). Histological analysis demonstrated lower histopathologic scores (**Fig 1E and 1F**). Additionally, BG-pretreated mice exhibited enhanced intestinal epithelial barrier integrity, as evidenced by the increased expression of tight junction proteins Zo-1 and Occludin (**Fig 1G and 1H**), and decreased circulating FITC-dextran levels (**Fig 1I**).

Acknowledging the long-lasting effects of BGTI(16), we further examined its long-term protective effects against DSS-induced colitis. Despite peripheral myeloid cells and monocytes returning to homeostasis four weeks post-BG treatment (**Fig S2A and S2B**), mice remained protected against DSS-induced colitis as demonstrated by body weight change and colon shortening (**Fig 1J and 1K**), and improved histological outcomes (**Fig S2C and S2D**). This BG-induced protection persisted for up to seven weeks (**Fig S2E and S2F**). These findings indicate that BG pretreatment effectively ameliorates DSS-induced colitis in mice, emphasizing the therapeutic potential of trained immunity in IBD management.

BG ameliorates colitis via enhanced myeloid cell activation independent of adaptive immunity

Given that BGTI has been reported to function independently of adaptive immunity(17, 18), we evaluated the effects of BG pretreatment in *Rag1* knockout mice (**Fig S3A-S3D**). Notably, BG pre-treatment remained effective in *Rag1*$^{-/-}$ mice, as evidenced by reduced body weight loss, colon

105 shortening, and improved histological outcomes (**Fig S3E-S3H**). These findings confirm that
106 BGTI-mediated protection is independent of adaptive immune responses, consistent with previous
107 findings demonstrating that adaptive immunity is dispensable for trained immunity.

108 To gain a comprehensive understanding of the molecular mechanisms underlying BG-mediated
109 protection, we performed RNA sequencing on colonic samples collected at multiple time points
110 following DSS administration. WGCNA identified the MEturquoise module emerged as the core
111 functional module, containing 5,015 genes whose expression exhibited significant co-regulation
112 following BG intervention (**Fig S4A**). And differential gene expression of genes within this
113 module was most significant on day 7 post-DSS treatment when comparing the BG-treated mice
114 to PBS controls (**Fig S4B**). GO analysis revealed significant enrichment in pathways related to
115 chemotaxis and leukocyte migration (**Fig 2A**). KEGG pathway enrichment analysis demonstrated
116 significant activation of cellular processes involved in phagocytic function (**Fig 2B**) Additionally,
117 the enrichment observed in WGCNA was further corroborated by whole-genome analysis of day 7
118 colitis samples, which also identified significant enrichment of pathways associated with
119 chemotaxis, leukocyte migration and phagocytic function (**Fig S4C and S4D**). Multiple analytical
120 approaches concurrently indicated that BG pretreatment not only enhances the recruitment of
121 immune cells but also promotes their functional activation, particularly with respect to phagocytic
122 capabilities.

123 To further investigate how BG pretreatment reprograms of intestinal myeloid cells, we performed
124 single-cell RNA-seq to characterize intestinal leukocytes populations on day 7 post-DSS treatment.
125 Unbiased clustering analysis identified multiple clusters of intestinal immune cells subsets,
126 including monocytes/macrophages (*Ly6c2*, *Ccr2* and *Adgre1*), dendritic (DC) (*Cst3* and *H2-Aa*),
127 neutrophils (*S100a8/a9* and *Ly6g*), B (*Cd79a Cd79b* and *Cd19*), Pre B (*Myl4* and *Mme*), CD4 T
128 (*Cd3d* and *Cd4*), CD8 T (*Cd3d* and *Cd8a*), natural killer (*Nkg7*), ILC2 (*Gata3* and *Il4*) and ILC3
129 (*Rorc* and *Il22*) cells (**Fig 2C and Fig S4E**). Importantly, the ratio of monocytes/macrophages and
130 neutrophils was elevated in the BG group (**Fig 2D**).

131 Single-cell RNA-sequencing data further demonstrated enhanced expression of innate pathogen

132 recognition receptors (*Syk*, *Nod1*, *Nod2*, *Tlr2* and *Tlr4*), efferocytosis (*Cd300lf*, *Axl*, *Mertk*, *Itgal*
133 and *Itgb7*), cytokines (*Il1b*, *Il1rn*, *Vegfa* and *Tgfb1*), chemokines (*Ccl2*, *Ccl6*, *Ccl9*, *Cxcl9*) and
134 chemokine receptors (*Ccr1*, *Ccr2*, *Cxcr4*) in intestinal monocytes/macrophages (**Fig 2E**). AUC
135 and KEGG analysis demonstrated significant enrichment pathways related to activation of innate
136 immune response and phagocytosis in monocytes/macrophages from BG-treated mice (**Fig 2F**
137 **and 2G**). These findings, corroborated by WGCNA analysis, strongly suggest that BG
138 pretreatment enhanced the recruitment and activation of myeloid cells, particularly
139 monocytes/macrophages, in the inflamed colon, thereby improving disease outcomes.

140 BG trained bone marrow monocytes protected against colitis via the Ccl2-Ccr2 141 axis

142 Drawing upon single-cell transcriptome analysis that reveals the proportional expansion and
143 functional reprogramming features of colonic monocyte/macrophage populations, in conjunction
144 with the observation of significantly upregulated peripheral monocytes following BG pretreatment
145 as depicted in **Fig S2B**. A hypothesis was formulated that BG exerts protective effects against
146 colitis via monocytes. To experimentally validate this hypothesis, we evaluated the role of
147 monocytes in *Ccr2* KO mice. Circulating Ly6C^{hi} monocytes were diminished in *Ccr2*$^{-/-}$ mice (**Fig**
148 **S5A and S5B**), corroborating the pivotal role of the Ccl2-Ccr2 axis in monocyte egression from
149 the bone marrow into circulation(19, 20). Notably, BG pretreatment failed to protect *Ccr2*$^{-/-}$ mice
150 from DSS-induced colitis, as evidenced by the lack of significant differences in body weight loss,
151 colon length, and epithelial permeability (**Fig 3A-E**).

152 In view of the fact that BG induces myelopoiesis through the modulation of hematopoietic stem
153 and progenitors cell compartments in the bone marrow via central trained immunity(21, 22). we
154 assessed whether transplantation of bone marrow cells from BG-pretreated donors could confer
155 resistance to DSS-induced colitis in naïve recipients (**Fig 3F**). At 6 weeks post-transplantation,
156 circulating myeloid cells were predominately derived from donor mice as indicated by the CD45.1
157 marker on circulating mononuclear cells (**Fig S5C**). Following DSS treatment, mice receiving
158 bone marrow cells from BG-pretreated donors exhibited significantly reduced body weight loss

159 (**Fig 3G**). However, no significant difference in colon length was observed (**Fig 3H and Fig S5D**).
160 Meanwhile, the percentage of circulating CD11b^{+} myeloid cells, neutrophils and Ly6C^{hi}
161 monocytes were increased (**Fig 3I and J**, **Fig S5E**).

162 To further assess the role of monocyte, we adoptively transferred bone marrow Ly6C^{hi} monocytes
163 sorted from control or BG-trained donor mice into *Ccr2*$^{-/-}$ recipient mice, which were then
164 subjected to DSS treatment (**Fig S5F and S5G**). Mice received BG-trained monocytes exhibited
165 reduced weight loss and colon shortening (**Fig 3K and 3L**). These findings suggest that
166 BG-trained Ly6C^{hi} Ccr2^{+} monocytes play a pivotal role in the alleviation of colitis.

167 BG-trained monocytes enhance innate immune activation and microbial control

168 To explore the heterogeneity and functional roles of monocytes and macrophages, we delved
169 deeper into the scRNA-seq data. By examining the expression of key signature genes, including
170 *Ly6c2*, *Ccr2*, *H2-Ab1*, *Runx3*, *Itgax*, *Adgre1*, *Cx3cr1* and *Cd209a*, we identified eight distinct
171 immune cell subsets: three monocyte subsets (Mono1-3) characterized by high *Ly6c2* and *Ccr2*
172 expression, four macrophage subsets (Macro1-4) defined by expression of *H2-Ab1*, *Runx3*, *Itgax*,
173 *Adgre1*, and *Cx3cr1*, and a dendritic cell subset (Cd209a^{+}DC) expressing integrin *Itgax* and C-type
174 lectin *CD209a* (**Fig 4A and Fig S6A**). Among macrophage subsets, Macro1 highly expressed
175 *Vegfa*, suggesting that may be a mucosal repair-promoting macrophage population. Macro2 was
176 enriched with tissue-resident macrophage signature genes (*Runx3*, *Dtx4*, *Cx3cr1*, *Hes1*). In
177 contrast, Macro3 and Macro4 deviated from the main cluster in cell clustering analysis, showing
178 significant heterogeneity. Macro3 was characterized by high *Ighm* expression, while Macro4
179 showed elevated *Cd4* expression. Both Macro2 and Macro4 exhibited higher *Il10* expression than
180 other monocyte/macrophage subsets, indicating their inflammation-regulatory functions.

181 The BG-treated group exhibited a significant increase in the proportions of Mono1, Mono2,
182 Macro1, and CD209a^{+}DCs, whereas higher proportions of Mono3 and Macro3 were observed in
183 the PBS group (**Fig 4B**). Given the strong enrichment of Mono1 and the reduction of Mono3
184 following BG treatment, we sought to further define the transcriptomic characteristics that
185 differentiate Mono1 from Mono3. GO enrichment analysis revealed that Mono1 was significantly
186 enriched in pathways regulating the activation of innate immune response (**Fig S6B**). KEGG
187 pathways analysis further identified enrichment in NOD-like receptor (NLR) signaling, Toll-like
188 receptor (TLR) signaling, and phagocytosis (**Fig 4C**). AUC analysis further confirmed the TLR

189 and NLR signaling pathways were significantly upregulated in Mono1 and Mono2 subsets of the
190 BG-pretreated group (**Fig S6C and S6D**). Additionally, antimicrobial humoral response pathway
191 was also upregulated in these two subclusters (**Fig S6E**). Cooperative activation of the pattern
192 recognition receptor (PRR) signaling axis and antimicrobial humoral response significantly
193 promotes the synthesis of antimicrobial peptides(23, 24). BG pretreatment significantly
194 upregulated genes encoding pattern recognition receptors (*Nod1*, *Nod2*, *Tlr2*, *Tlr4*) and
195 antimicrobial effector molecules (*S100a8*, *S100a9*, *Lcn2* and *Defb1*) in the colon on day 7 of
196 colitis (**Fig 4D**). Furthermore, antimicrobial genes *S100a8* and *Defa1* were highly expressed in the
197 BG group as validated by qPCR analysis (**Fig S6F**). These genes upregulation suggest a potential
198 link between trained immunity and enhanced microbial control. Consistently, gene signatures
199 associated with bacterial defense responses were prominently enriched in the BG-treated group
200 (**Fig 4E**).

201 To investigate the epigenetic basis for this sustained transcriptional reprogramming, we reanalyzed
202 publicly available ATAC-seq data from hematopoietic stem cells (HSCs) of BG-trained mice
203 (CRA014389). This analysis revealed that BG training reshaped the epigenomic landscape, with
204 pronounced chromatin opening at promoters and distal intergenic regulatory loci (Fig S7A, B).
205 Functional annotation of these primed regions showed significant enrichment for immune
206 processes, including leukocyte migration and chemotaxis (Fig S7C), as well as pathways like
207 chemokine signaling (Fig S7D). Crucially, promoter-centric analysis highlighted the enrichment of
208 defense response to bacterium (Fig S7E), and locus-specific examination confirmed BG-induced
209 chromatin remodeling upstream of key antimicrobial effectors, including Gbp2, Gbp5, S100a8,
210 and Nos2 (Fig S7F). This demonstrates that BG establishes a permissive epigenetic architecture in
211 progenitor cells, priming the expression of immune and antibacterial programs.

212 Consistent with this primed epigenetic state, we observed a significant enrichment of the IFN-γ
213 response pathway (Fig S6G) and a specific upregulation of Guanylate-binding protein (Gbp) genes
214 (Gbp2, Gbp3, Gbp5, Gbp7) in the Mono1 and Mono2 subsets (Fig 4F). Previous studies have
215 demonstrated that GBPs as intracellular effectors induced by IFNγ and LPS to promote

216 antibacterial defense(25, 26). GBP-deficient mice exhibit significantly increased susceptibility to
217 Salmonella typhimurium infection(27-29). We then performed intestinal Salmonella typhimurium
218 infection to assess whether BG pretreatment enhances microbial control in the gut (Fig 4G). As
219 expected, BG pretreatment significantly protected mice from lethal Salmonella Typhimurium
220 infection, suggesting that BG-induced trained immunity enhances mucosal defenses against gut
221 microbial infections (Fig 4H).

222 Taken together, these results reinforced our bulk RNA-seq findings, indicating that BG
223 pretreatment induces a specific monocyte subcluster with enhanced innate activation and
224 phagocytic capacity, facilitating more efficient control of the breaching microbiome associated
225 with DSS-induced leaky gut.

226 BG-mediated reprogramming of myeloid differentiation trajectories balances 227 inflammation and enhances mucosal repair in colitis

228 While BG-induced trained immunity is characterized by enhanced pro-inflammatory cytokine
229 production and increased bactericidal capacity(14), excessive pro-inflammatory cytokines release
230 may exacerbate colitis progression. To balance heightened cytokine production without inducing
231 overwhelming immunopathology, we hypothesized that BG pretreatment might involve feedback
232 loops that modulate the inflammation while preserving enhanced phagocytic capacity.

233 To investigate this, we analyzed previously obtained bulk colonic RNA-seq data, focusing on
234 genes associated with anti-inflammatory and regulatory functions. On day 7 of colitis, BG
235 pretreatment significantly upregulated genes encoding immunomodulatory factors (*Il4*, *Il10*, *Il11*
236 and *Il33*), signaling inhibitors (*Socs1*, *Socs3*), and differentiation regulators (*Csf1*, *Csf1r*, *Stat3* and
237 *Stat6*) (**Fig S8A**) The upregulation of *Socs1* and *Socs3* was further corroborated by scRNA-seq
238 data, which showed increased expression of these genes in the Mono1 and Mono2 subclusters (**Fig
239 S8B**). As members of the suppressor of cytokine signaling (SOCS) family, SOCS1 and SOCS3
240 inhibit excessive JAK-STAT signaling activation via negative feedback regulation(30-32).
241 Moreover, coordinated activation of the monocyte/macrophage differentiation regulatory network
242 (*Csf1r*, *Nr4a2*, *Irf8*, *Klf4*) suggests that BG may induce the differentiation of regulatory-phenotype

243 macrophage subsets by reprogramming myeloid developmental trajectories, thereby modulating
244 inflammatory responses.

245 To further investigate whether BG pretreatment reprograms monocyte-to-macrophage
246 differentiation, we analyzed the day7 RNA-seq data, which revealed significant enrichment of
247 myeloid leukocyte differentiation pathway (**Fig S8C**). Additionally, Single-cell trajectory analysis
248 further revealed that Macro1 and Macro2 differentiated from Mono2 and Mono3, respectively
249 (**Fig 5A**). BG training significantly accelerated the differentiation kinetics of Mono3 into Macro1,
250 which may underlie the reduced frequency of the Mono3 subset in the BG group. Coupled with
251 the gene expression signatures in **Fig S6A**, Macro1 shares similarities with Macro2 in marker
252 gene expression, and the differentiated Macro1 subset could further differentiate into the
253 tissue-resident macrophage Macro2 subset (**Fig 5B**).

254 Furthermore, we observed that the expression levels of *Ccr2* and *Ly6c2* decreased from Mono1 to
255 Macro2, while *H2-Ab1* and *Cx3cr1* progressively increased, particularly in macrophages (**Fig 5C**).
256 Since Cx3cr1 upregulation is a hallmark of circulating monocytes migrating to the intestinal
257 lamina propria and undergoing macrophage differentiation(33), we used *CX3CR1-GFP* reporter
258 mice to monitor the monocyte-to-macrophage transition in the DSS colitis model. In circulating
259 leukocyte subsets, the total percentage of $CD11b^+$ myeloid cells was higher in BG-pretreated mice
260 compared to controls (**Fig S9A-C**). A similar trend was observed in neutrophils (**Fig S9D and**
261 **S9E**). While the initial monocyte percentage was higher in the BG group, no significant difference
262 was observed the two groups on day 7 post-DSS treatment (**Fig 5D and S9F**), suggesting that
263 circulating monocytes in BG-pretreated mice had extravasated into the intestinal tissue.
264 Meanwhile, the percentage of colonic $CD11b^+$ myeloid cells and neutrophils was increased in the
265 BG-pretreated group (**Fig S10A-C**).

266 We further defined monocyte/macrophage populations from P1 to P6 based on the expression of
267 CD11b, CX3CR1-GFP, Ly6C, and MHCII. P1 to P3 were gated from
268 $CD11b^+$&$CX3CR1\text{-}GFP^-$&$Ly6G^-$ cells. While P1 ($Ly6C^+$&$MHCII^-$) and P3 ($Ly6C^-$&$MHCII^+$)
269 were comparable between group, P2 ($Ly6C^+$&$MHCII^+$) was increased in BG-pretreated mice (**Fig**

5E). P4 to P6 are gating from CD11b^{+}&CX3CR1-GFP^{+} cells and further separate by the expression of Ly6C and MHCII. P4 (Ly6C^{+}&MHCII^{-}) as infiltrating monocytes gaining CX3CR1 expression. P5 (Ly6C^{+}&MHCII^{+}) is regarded as intermediate transitory immature macrophage and P6 (Ly6C^{-}&MHCII^{+}) is considered as mature macrophage as it completely loss expression of Ly6C and highly express MHCII. BG pretreatment led to an increase in P5 level (**Fig 5F**). The increase of P2 and P5 in BG group in line with the decrease of monocytes at day 7 in circulation post DSS treatment, suggesting that BG trained monocytes have higher capacity to infiltrate into the damaged colon and undergo macrophage differentiation.

Previous WGCNA analysis suggested that BG pre-treatment upregulated the focal adhesion pathway, which may enhance tissue repair mechanisms (**Fig 2B**). Consistent with this, we observed increased expression of genes involved in wound healing and tissue repair, such as *Mmp*-related genes, *Spon1*, *Notch1*, *Notch2*, *Tgfb*, *Fgf1*, *Fgf2*, *Col1a1*, *Col1a2*, *and Fn1* in the BG-treated group on day 7, followed by a rapid decline by day 12. In contrast, the PBS group exhibited a much milder induction of these genes, with several genes remaining at comparable levels between day 7 and day 12 (**Fig 5G**). This led us to hypothesize that the upregulated monocytes and macrophages in the BG-treated group might exhibit enhanced expression of tissue repair-associated genes. As expected, the expression of *Spon1* and *Mmp14*, which promote the mucosal repair was increased in Mono2, Macro1, and Macro2 (**Fig 5H and 5I**). These findings suggest that BG pretreatment indeed induced monocyte and macrophage subsets with enhanced tissue repair capacity.

291 **Discussion**

292 Trained immunity, a non-antigen-specific form of innate immunological memory, enables rapid
293 host defense mobilization upon pathogen challenge(34, 35). In inflammatory bowel disease, gut
294 microbial dysbiosis manifests as reduced α-diversity, diminished commensal taxa (e.g.,
295 *Faecalibacterium prausnitzii*), and pathobiont expansion (e.g., *Enterobacteriaceae*,
296 *adherent-invasive Escherichia coli*), which may compromise intestinal barrier integrity and
297 precipitate microbial translocation(36-38). Additionally, the long-term use of immunosuppressants
298 and biologics in IBD patients elevates infection susceptibility, rendering the microbial-controlling
299 properties of trained immunity a viable therapeutic strategy for IBD(39). However, Excessive or
300 sustained immune activation could trigger chronic inflammatory cascades and provoke
301 autoimmune tissue damage through aberrant immune recognition, as observed in conditions such
302 as rheumatoid arthritis and cardiovascular diseases(9, 40-42). However, the functional correlation
303 between trained immunity and colitis remains unclear, and how to apply trained immunity to
304 colitis treatment represents an urgently unresolved scientific question.

305 Here, we demonstrated that BG-induced trained immunity confers cross-pathogen protective
306 effects using a lethal *Staphylococcus aureus* infection model, while failing to induce intestinal
307 inflammation under conditions of an intact mucosal barrier. Further investigations revealed that
308 BG effectively attenuated dextran sulfate sodium (DSS)-induced colitis upon secondary challenge.
309 BG pretreatment conferred long-term protection against DSS-induced colitis, with benefits lasting
310 for at least two months after the peripheral myeloid cell populations returned to baseline levels.
311 Bone marrow transplantation experiments confirmed that BG-induced trained immunity persists
312 within hematopoietic progenitors, leading to durable reprogramming of peripheral monocytes.
313 This long-term effect is likely supported by epigenetic modifications in hematopoietic cells, as
314 reported in previous studies(21, 43). These findings highlight the potential of BG-induced trained
315 immunity in establishing long-lasting immune memory, which could be leveraged to achieve
316 sustained therapeutic effects in IBD.

317 The conventional understanding of IBD pathogenesis has long posited that abnormal immune
318 activation is central to disease development and progression. This paradigm has predominantly
319 focused on the role of adaptive immunity, particularly the dysregulation of Th17 and Treg
320 functions over the past decades(44-46). However, our results suggest that BG-induced protection

321 is independent of adaptive immune responses. Even in *Rag1*$^{-/-}$ mice, which lack adaptive immunity,
322 BG pretreatment significantly improved DSS-induced colitis outcomes. *Rag1*$^{-/-}$ mice retain ILCs
323 (including ILC3s), which promote mucosal repair via IL-22 production(47). While BG-induced
324 ILC activation remains untested, our monocyte adoptive transfer experiments show monocytes
325 alone alleviate colitis—suggesting a dominant, but not exclusive, role for monocytes/macrophages.
326 ILC contributions cannot be ruled out and warrant further investigation.

327 In DSS-induced colitis, epithelial barrier disruption facilitates microbiota translocation across the
328 mucosal epithelium, triggering inflammatory responses mediated by innate cells(38, 48, 49). We
329 identified monocytes as key mediators of BG-induced protection against DSS-induced colitis, as
330 demonstrated by experiments using *Ccr2*$^{-/-}$ mouse models and monocyte transfer studies. BG
331 pretreatment enriched Ly6C^{hi}CCR2^{+} monocytes, which exhibited enhanced antimicrobial
332 capabilities, as revealed by scRNA-seq. Ly6C^{hi}CCR2^{+} monocytes displayed higher levels of
333 antimicrobial receptors like NOD2, TLR4 and GBP-related gene. Guanylate-binding protein (GBP)
334 enhances *Salmonella* clearance by promoting inflammasome activation and intracellular bacterial
335 elimination, particularly through disrupting *Salmonella*-containing vacuoles and inducting
336 pyroptosis(27, 50). Our finding revealed that BG pretreatment increased resistance to *Salmonella*
337 *typhimurium* infection. As inflammation and infection is partially controlled, monocytes can
338 differentiate into macrophage subsets with anti-inflammatory and tissue repair functions, secreting
339 cytokines such as IL-10, TGF-β and VEGF to promote inflammation resolution and tissue
340 repair(51, 52).

341 Previous studies have underscored the essential role of circulating Ly6C^{hi} monocytes in
342 replenishing intestinal macrophages(53, 54). During colitis and infection, these monocytes are
343 rapidly recruited to injured colonic tissues, where they differentiate into Cx3cr1^{+} macrophages.
344 We also observed that these monocytes exhibited enhanced migratory capabilities, enabling them
345 to infiltrate inflamed tissues and differentiate into CX3CR1^{+} macrophages. These macrophages
346 contribute to mucosal repair by clearing pathogens such as *Salmonella* and promoting epithelial
347 regeneration(55). Single-cell trajectory analysis further showed that BG training promoted the

348 differentiation of Macro1 into Macro2, which is consistent with the dynamic process of
349 monocyte-to-mature macrophage conversion observed in *CX3CR1-GFP* reporter mice.
350 Maintaining a balance between inflammatory monocytes, differentiated macrophages, and
351 tissue-resident macrophages is critical for resolving inflammation, promoting tissue repair(33, 56).
352 These findings suggest that BG not only augments monocyte antimicrobial functions but also
353 facilitates their differentiation into macrophages, enhancing their ability to recognize, phagocytose,
354 and eliminate bacteria while promoting tissue repair. This dual function likely strengthens the
355 intestinal barrier, mitigates inflammation, and supports gut homeostasis.

356 Notably, our findings align with emerging evidence that trained immunity (TI) is not a uniform
357 biological process but encompasses distinct functional programs shaped by the initiating stimulus
358 and contextual cues—including immunoregulatory and tissue-reparative responses. Yang Li et al
359 have identified discrete monocyte/macrophage subpopulations following TI induction, such as
360 cytokine-chemokine dual-high (MCI) and chemokine-high (MC) subsets, which exhibit distinct
361 pathway enrichments and disease associations(57). Consistent with this, β-glucan (BG), the TI
362 inducer in our study, has been shown to drive a specific subset of macrophages with M2-like
363 phenotypic traits (e.g., high CD206 expression, increased IL-10 secretion) while retaining potent
364 antimicrobial capabilities (e.g., bacterial killing, pro-inflammatory cytokine release upon LPS
365 stimulation)—reflecting an immunoregulatory TI program that balances pathogen clearance and
366 inflammation resolution(58). Furthermore, BG-induced TI has been reported to inhibit NLRP3
367 inflammasome activation via blocking K^+ efflux and mitochondrial ROS generation, highlighting
368 its context-dependent anti-inflammatory potential in autoinflammatory diseases(59)—a
369 mechanism that may contribute to its protective effects in colitis by limiting excessive intestinal
370 inflammation. Our findings of BG-induced protection against DSS colitis, characterized by
371 enhanced microbial clearance and accelerated mucosal repair without exacerbating inflammation,
372 represent a paradigmatic example of such context-dependent, reparative TI programs. This aligns
373 with the broader understanding that TI can be tailored to elicit tissue-protective effects when
374 triggered by appropriate stimuli, as demonstrated by BG's ability to prime myeloid cells for both
375 antimicrobial defense and tissue repair(60). Together, these observations place our work within the

376 growing framework of TI functional heterogeneity, emphasizing that the biological outcome of TI
377 is dictated by the interplay between the inducing stimulus, target cell type, and local
378 microenvironment—an insight that further clarifies the mechanism by which BG-induced TI
379 confers colitis protection.

380 In the clinical exploration of IBD treatment, novel therapies based on cellular regeneration
381 (intestinal organoid transplantation) and fecal microbiota transplantation (FMT) are emerging as
382 critical avenues to overcome the limitations of conventional pharmacotherapies(61-63). Given the
383 efficacy of BG-induced trained immunity in alleviating DSS-induced colitis, this approach holds
384 significant promise as a novel therapeutic strategy for IBD treatment. We transferred
385 BG-preconditioned monocytes which significantly alleviated clinical symptoms, including weight
386 loss and colon shortening, demonstrating the potential of cell-based therapies (**Fig S11A-C**).

387 In conclusion, BG confers long-term colitis amelioration through trained immunity by
388 reprogramming bone marrow-derived monocytes. Mechanistically, BG enhances monocyte
389 chemotaxis and antimicrobial functionality activation, enabling efficient microbial containment.
390 Crucially, this trained state establishes self-regulating circuits, engaging in negative feedback
391 regulation of excessive immune responses, while accelerated $CX3CR1^+$ macrophage
392 differentiation facilitates mucosal repair. These findings establish a foundation for leveraging
393 trained immunity as a therapeutic strategy for IBD, highlighting the potential of BG in modulating
394 intestinal immunity and restoring gut homeostasis.

395 Limitations

396 Although our reanalysis of publicly available ATAC-seq datasets (data available from
397 CRA014389) targeting monocytes confirmed BG-induced chromatin accessibility enrichment at
398 antibacterial defense related genomic regions, direct mechanistic evidence for epigenetic and
399 metabolic profiling in our colitis model remains lacking, and we plan to pursue as future work.
400 Moreover, the functional role of $CX3CR1^+$ macrophages remained correlative. Despite
401 transcriptional evidence of repair-related gene expression and phenotypic correlation with colitis
402 resolution, we lack direct causal data due to the unavailability of specific tools for this subset. The

403 fate of adoptively transferred monocytes was not directly traced. Current evidence remains
404 correlative and requires validation through future lineage-tracing studies.

405 **Materials and Methods**

406 **Animals**

407 C57BL/6J wild-type male mice (6-8weeks) were purchased from Xiamen University Laboratory
408 Animal Center. *Rag1*$^{-/-}$ and *CX3CR1-GFP* mice were generously provided by Dr. Kairui Mao and
409 Dr.Xiaofen Chen from Xiamen University, respectively. *Ccr2*$^{-/-}$ mice were kindly provided by Dr.
410 Shih-Chin Cheng from Xiamen University. Mice were maintained under specific pathogen-free
411 conditions. All animal protocols were reviewed and approved by the Institutional Animal Care and
412 Use Committee of Xiamen University.

413 **In vivo beta-glucan (BG) training and DSS colitis model**

414 Mice were i.p. injected with one dose of BG (1 mg) on day -7/-49, Then, Mice received 3%
415 indicated DSS (36,000 to 50,000 molecular weight; MP Biomedicals) in their drinking water for 5
416 days, followed by 2 days or 7 days of distilled water without DSS. Control animals received
417 distilled water for the entire period. Mice were monitored every day from day 0 for body weight
418 until day 7 or 12.

419 **Histology**

420 Colons were collected from sacrificed mice at the end of each treatment schedule, as described
421 above, colon was fixed with 4% paraformaldehyde and embedded in Paraffin. Tissue sections (5
422 μm) were prepared, deparaffinized, and stained with hematoxylin and eosin. With minor
423 modifications, by assessing mucosa thickening, inflammatory cells, and submucosa cell
424 infiltration. Each criterion was scored as 0-4, and the sum of each score was defined as the
425 histological score. Histological scores were assigned by experimenters "blinded" to sample
426 identity.

427 **Coloscopy**

428 A coloscopy system (ENDOCAM® Logic HD, RICHARD WOLF) was used to monitor the
429 severity of DSS-induced colitis. After an 8-hour fast, we administered isoflurane (RWD, Co. Ltd.)
430 and applied glycerin to the anus for smooth insertion.

431 **In vivo intestine permeability assay**

432 Age and sex-matched mice were orally administered with 0.6 mg/g body weight of an 100 mg/ml
433 solution of FITC-dextran (FD4, Sigma). 5 hours later, retro-orbital blood was collected from each
434 mouse. Serum was prepared by allowing the blood to clot by leaving it undisturbed overnight at
435 4°C and then subsequently centrifuged at 5000 rpm for 10 minutes. Dilutions of FITC-dextran in
436 PBS and separately in pooled mouse serum were used as a standard curve. Absorbance of 50 µl
437 serum was measured at microplate reader with excitation and emission filters set at 490 and 530
438 nm, respectively. Experiments were performed at least two independent times each in triplicate.

439 **RNA extraction and real-time PCR**

440 Total RNA was extracted from colon tissue previously washed from luminal content. Samples
441 were homogenized in TRIZOL. Homogenized tissues were then added with chloroform in order to
442 separate RNA from genomic DNA and proteins. RNA isolation and purification required
443 isopropanol (RNA precipitation) and 70% ethanol (RNA wash). Total RNA was resuspended in
444 Nuclease-free water. Subsequently, 1 µg of RNA was reverse-transcribed using the Hifair® ll lst
445 Strand cDNA Synthesis SuperMix for qPCR (gDNA digester plus) following manufacturer's
446 instructions. cDNA was analysed through quantitative Real-Time PCR.

447 **Isolation of cells from lamina propria**

448 To isolate lamina propria mononuclear cells (lamina propria MCs), extraintestinal fat tissue was
449 carefully removed and colons were then flushed of their luminal content with physiologic solution,
450 opened longitudinally and cut into 1 cm pieces. Epithelial cells and mucus were removed by
451 incubation with 10 mL of D-Hank's balanced salt solution (containing EDTA and DTT, free of
452 $Ca2^{+}$ and $Mg2^{+}$) for 20 minutes at 37°C at 200 rpm in a constant temperature shaker. Colon pieces
453 were then digested in Hank's (with $Ca2^{+}$ and $Mg2^{+}$) containing 0.5 mg/ml Collagenase IV and 15
454 µg/ml DNase I, for 40 min at 37°C shaking at 200 rpm. The remaining cells were centrifuged and
455 resuspended in FACS buffer (1% FBS, 2 mM EDTA in PBS).

456 **Bone Marrow Transplantation**

457 Wild type CD45.2 mice were subjected to 8 Gy irradiation (RAD SOURCE, RS2000). These
458 irradiated recipients were then divided into three groups: a sham-transplant control group that
459 received an intravenous injection of PBS alone, a control BMT group that received bone marrow
460 cells from naïve CD45.1 donors, and a BG-trained BMT group that received bone marrow cells
461 from CD45.1 donors pretreated with β-glucan. Bone marrow cells were harvested from the femurs
462 of CD45.1 wild-type or BG-trained donor mice. A total of 1×10^7 bone marrow cells from the
463 respective donors were transferred to the irradiated CD45.2 recipients via tail-vein injection.
464 Successful engraftment was confirmed by flow cytometric analysis of donor-derived ($CD45.1^{+}$)
465 cells in peripheral blood (Fig. S5C). Six weeks post-transplantation, mice were administered 2.5%
466 DSS in drinking water to induce colitis and were monitored daily until day 12.

467 **Adoptive transfer of bone marrow monocytes**

468 BG trained mice were sacrificed, and the femurs were used to harvest bone marrow cells, Bone
469 marrow cells were stained with the following panel: Biotin antibody (B220, CD4, CD8, NK1.1,
470 Ly6G), Live/dead (Cat. L34976, Invitrogen), CD45 (Cat. 45-0451-82, Clone. 30-F11, ebioscience),
471 CD11b (Cat. 48-0112-82, Clone. M1/70, ebioscience), Ly6C (Cat. 128016, Clone. HK1.4,
472 Biolegend). Biotin-labeled lineage antibodies were used to stain bone marrow cells at 4℃ for 20
473 min and then incubated with fluorescence conjugated streptomycin together with other surface
474 protein antibodies for another 20 min. $Ly6C^{hi}$ monocytes were sorted to > 97% purity using a BD
475 Aria III cell sorter.

476 **RNA-seq**

477 RNA was extracted from colon LPLs of individual mice. RNA integrity was assessed using the
478 RNA Nano 6000 Assay Kit of the Bioanalyzer 2100 system (Agilent Technologies, CA, USA).
479 The clustering of the index-coded samples was performed on a cBot Cluster Generation System
480 using TruSeq PE Cluster Kit v3-cBot-HS (Illumia) according to the manufacturer's instructions.
481 The library was sequenced on an Illumina Novaseq platform and 150 bp paired-end reads were
482 generated.

483 **scRNA-seq**

484 Isolated lamina propria mononuclear cells, sample from three mice were pooled together and
485 analyzed per condition. For scRNA-seq of Colon $CD45^+$ cells were sorted by BD Arial III. These
486 cells were barcoded with 10× Cellplex oligos before being encapsulated using the 10X Chromium
487 3′ Reagent Kits v3 according to manufacturer's instructions.

488 **RNA-seq data processing and analysis**

489 Raw data of fastq format were quality checked through fastqc software. Gencode and gene model
490 annotation files were downloaded from genome (mm10) website directly. Index of the gencode
491 was built using Hisat2 v2.1.0 and paired-end clean reads were aligned to the gencode using Hisat2
492 v2.1.0. For differential expression analysis, raw count data (generated via featureCounts) were
493 used as input for DESeq2, with differential genes filtered by |fold change| ⩾ 2 and adjusted $P <$
494 0.05. FPKM (Fragment per kilobase per million) values were only used for visualization purposes
495 (e.g., heatmaps, clustering analyses), not for between-sample statistical comparisons. Weighted
496 correlation network analysis (WGCNA) was perform using an R package from horvath. All
497 differentially expressed genes were plotted with the "pheatmap" and "ggplot2" R packages. For
498 KEGG enrichment analysis, p-value < 0.05 was used as a threshold to determine significant
499 enrichment for gene sets with the "clusterProfiler" R package.

500 **scRNA-seq data processing and analysis**

501 Raw sequencing data was processed and aligned mm10 mouse reference genome with CellRanger
502 (10× Genomics) v 7.2.0. Resulting filtrated matrices (count matrices) of molecular counts were
503 used as input for further processing with Seurat package V5.0.1running under R studio. First,
504 quality control was performed to create Seurat object with min features > 200 and removal of cells
505 having < 200 or > 8000 expressed genes or > 5% mitochondrial counts. The total number of
506 recovered cells was mentioned before. Variable features using FindVariableFeatures (using RNA
507 and vst as an assay and selection method as parameters) and normalization using

normalization.method = "LogNormalize", scale.factor = 10000 were performed . This integrated data is scaled using ScaleData function using all genes and “RNA” as assay method.

Doublet cells were filtered by DoubletFinder v3. Principal Component Analysis was performed on variable features using RunPCA and first 30 PCs were chosen. The nearest neighbors using the FindNeighbors(dims=1:12) and FindClusters(resolution=0.8) function. For visualization, the non-linear dimensional reduction such as UMAP analysis was using RunUMAP function from Seurat. To calculate pseudotime based on the Mono/Marco subset data using the monocle3.

ATAC-seq data analysis

The ATAC-seq data were obtained from the CNCB (China National Center for Bioinformation) under accession number CRA014389. Quality control was performed using FastQC. The paired-end reads were then aligned to the mouse reference genome (mm10) using Bowtie2 with the parameters: -k 1 -D 20 -R 3 -N 1 -L 20 -i S,1,0.50 -X 2000. The aligned reads were converted to sorted BAM files using Samtools. Peak calling was conducted with MACS2 using a q-value threshold of 0.05, a model fold range of 5-50, and the "keep-dup all" option to retain all tags. Peak quantification was performed using Bedtools and normalized to reads per kilobase per million mapped reads (RPKM). Visualization files in BigWig format were generated using Deeptools. The identified peaks were annotated using the ChIPseeker package, and pathway analysis was carried out with the ClusterProfiler package. Gene Set Enrichment Analysis (GSEA) was performed using the MSigDB database (version v2022.1.Mm).

Statistical Analysis

Statistical analyses were conducted using GraphPad Prism version 9.0 and R statistical software (version 4.2.2, R Foundation for Statistical Computing). Data were analyzed using a two-tailed Student’s *t*-test. Multiple-group comparisons were performed using one-way or two-way analysis of variance (ANOVA) followed by Tukey’s multiple-comparisons test. Survival data were assessed using Kaplan-Meier survival plots, followed by the log-rank test. Significant differences were indicated by an asterisk ($p < 0.05$).

Acknowledgments:

We thank the staff of Xiamen University Laboratory Animal Center. Special thank to Prof. Kairui Mao and Prof. Xiao-fen Chen for generously providing mice. We appreciate the help of Dr. Jia Zhang and other staff from Prof. Shih-Chin Cheng's laboratory during the study.

Author contributions:

Y.Y.L. designed and performed the experiments, analyzed the data and wrote the paper; Y.Y.F., Q.X.G. and Q.Y. C. analyzed the data, wrote the paper, and supervised the study. Y.Q.H., L.W., H.X.S., E.M.C., Q.Y.X., Y.C., Q.Q.F., L.L.L provided advice and oversaw a portion of the work. J.L.R., S.-C.C., H.Z.X. conceived the idea, secured funding, supervised the study, helped in data interpretations, revised drafts of manuscript; supervised overall project. All authors reviewed and approved the final version of the manuscript.

Ethics statements

Patient consent for publication: Not applicable.

Ethics approval

All animal protocols were reviewed and approved by the Institutional Animal Care and Use Committee of Xiamen University.

Funding:

This project was supported by National Key R&D Program of China (2022YFA1304000), National Natural Science Foundation of China (82300630&32161133020), Healthcare System Youth Backbone Talent Training Project of Fujian Province(2023GGB09), Municipal Natural Science Foundation of Xiamen (3502Z20227271), Foundation of State Key Laboratory of Vaccines for Infectious Diseases, Xiang An Biomedicine Laboratory (2023XAKJ0101012), Medical and Health Key Project of Xiamen (3502Z20204007).

Data availability statement

All data relevant to the study are included in the manuscript or uploaded as online supplemental

560 information. Sequencing data have been deposited to the GEO with accession number GSE285859
561 (single cell RNA-seq), GSE285860 (RNA-seq).
562
563

Reference

1. Kobayashi T, Siegmund B, Le Berre C, Wei SC, Ferrante M, Shen B, et al. Ulcerative colitis. Nat Rev Dis Primers. 2020;6(1).
2. Dolinger M, Torres J, Vermeire S. Crohn's disease. Lancet. 2024;403(10432):1177-91.
3. Zhang F, Aschenbrenner D, Yoo JY, Zuo T. The gut mycobiome in health, disease, and clinical applications in association with the gut bacterial microbiome assembly. Lancet Microbe. 2022;3(12):E969-E83.
4. Abraham C, Medzhitov R. Interactions Between the Host Innate Immune System and Microbes in Inflammatory Bowel Disease. Gastroenterology. 2011;140(6):1729-37.
5. Jostins L, Ripke S, Weersma RK, Duerr RH, McGovern DP, Hui KY, et al. Host-microbe interactions have shaped the genetic architecture of inflammatory bowel disease. Nature. 2012;491(7422):119-24.
6. Wehkamp J, Harder J, Weichenthal M, Schwab M, Schäffeler E, Schlee M, et al. NOD2 (CARD15) mutations in Crohn's disease are associated with diminished mucosal α-defensin expression. Gut. 2004;53(11):1658-64.
7. Watanabe T, Kitani A, Murray PJ, Strober W. NOD2 is a negative regulator of Toll-like receptor 2-mediated T helper type 1 responses. Nat Immunol. 2004;5(8):800-8.
8. Noguchi E, Homma Y, Kang XY, Netea MG, Ma XJ. A Crohn's disease-associated NOD2 mutation suppresses transcription of human IL10 by inhibiting activity of the nuclear ribonucleoprotein hnRNP-A1. Nat Immunol. 2009;10(5):471-9.
9. Netea MG, Joosten LAB, Latz E, Mills KHG, Natoli G, Stunnenberg HG, et al. Trained immunity: A program of innate immune memory in health and disease. Science. 2016;352(6284).
10. Netea MG, Domínguez-Andrés J, Barreiro LB, Chavakis T, Divangahi M, Fuchs E, et al. Defining trained immunity and its role in health and disease. Nat Rev Immunol. 2020;20(6):375-88.
11. Ding CL, Shrestha R, Zhu XJ, Geller AE, Wu SZ, Woeste MR, et al. Inducing trained immunity in pro-metastatic macrophages to control tumor metastasis. Nat Immunol. 2023;24(2):239-+.
12. Jeyanathan M, Vaseghi-Shanjani M, Afkhami S, Grondin JA, Kang ALS, D'Agostino MR, et al. Parenteral BCG vaccine induces lung-resident memory macrophages and trained immunity via the gut-lung axis (vol 23, pg 1687, 2022). Nat Immunol. 2023;24(6):1049-.
13. Zhu YH, Gao QX, Zhang J, Cheng Y, Yang SZ, Xu R, et al. Persistent bone marrow hemozoin accumulation confers a survival advantage against bacterial infection via cell-intrinsic Myd88 signaling. Cell Rep. 2024;43(10).
14. Moorlag SJCFM, Khan N, Novakovic B, Kaufmann E, Jansen T, van Crevel R, et al. β-Glucan Induces Protective Trained Immunity against Mycobacterium tuberculosis Infection: A Key Role for IL-1. Cell Rep. 2020;31(7).
15. Cheng SC. mTOR- and HIF-1α-mediated aerobic glycolysis as metabolic basis for trained immunity (vol 346, aaa1503, 2014). Science. 2014;346(6211):821-.
16. Kalafati L, Kourtzelis I, Schulte-Schrepping J, Li XF, Hatzioannou A, Grinenko T, et al. Innate Immune Training of Granulopoiesis Promotes Anti-tumor Activity. Cell. 2020;183(3):771-+.
17. Netea MG, Quintin J, van der Meer JWM. Trained Immunity: A Memory for Innate Host Defense. Cell Host Microbe. 2011;9(5):355-61.

18. Quintin J, Saeed S, Martens JHA, Giamarellos-Bourboulis EJ, Ifrim DC, Logie C, et al. Infection Affords Protection against Reinfection via Functional Reprogramming of Monocytes. Cell Host Microbe. 2012;12(2):223-32.
19. Tsou CL, Peters W, Si Y, Slaymaker S, Aslanian AM, Weisberg SP, et al. Critical roles for CCR2 and MCP-3 in monocyte mobilization from bone marrow and recruitment to inflammatory sites. J Clin Invest. 2007;117(4):902-9.
20. Geng HX, Chen LN, Tang J, Chen YA, Wang L. The Role of CCL2/CCR2 Axis in Cerebral Ischemia-Reperfusion Injury and Treatment: From Animal Experiments to Clinical Trials. Int J Mol Sci. 2022;23(7).
21. Mitroulis I, Ruppova K, Wang BM, Chen LS, Grzybek M, Grinenko T, et al. Modulation of Myelopoiesis Progenitors Is an Integral Component of Trained Immunity. Cell. 2018;172(1-2):147-+.
22. Chavakis T, Mitroulis I, Hajishengallis G. Hematopoietic progenitor cells as integrative hubs for adaptation to and fine-tuning of inflammation. Nat Immunol. 2019;20(7):802-11.
23. Muniz LR, Knosp C, Yeretssian G. Intestinal antimicrobial peptides during homeostasis, infection, and disease. Front Immunol. 2012;3.
24. Duarte-Mata DI, Salinas-Carmona MC. Antimicrobial peptides′ immune modulation role in intracellular bacterial infection. Front Immunol. 2023;14.
25. Sweet MJ, Ramnath D, Singhal A, Kapetanovic R. Inducible antibacterial responses in macrophages. Nat Rev Immunol. 2024.
26. Pilla DM, Hagar JA, Haldar AK, Mason AK, Degrandi D, Pfeffer K, et al. Guanylate binding proteins promote caspase-11-dependent pyroptosis in response to cytoplasmic LPS. P Natl Acad Sci USA. 2014;111(16):6046-51.
27. Man SM, Karki R, Sasai M, Place DE, Kesavardhana S, Temirov J, et al. IRGB10 Liberates Bacterial Ligands for Sensing by the AIM2 and Caspase-11-NLRP3 Inflammasomes. Cell. 2016;167(2):382-+.
28. Santos JC, Broz P. Sensing of invading pathogens by GBPs: At the crossroads between cell-autonomous and innate immunity. J Leukocyte Biol. 2018;104(4):729-35.
29. Meunier E, Dick MS, Dreier RF, Schürmann N, Broz DK, Warming S, et al. Caspase-11 activation requires lysis of pathogen-containing vacuoles by IFN-induced GTPases. Nature. 2014;509(7500):366-+.
30. Yuan FF, Peng W, Yang YY, Xu JQ, Liu YD, Xie Y, et al. Endothelial progenitor cell-derived exosomes promote anti-inflammatory macrophages via SOCS3/JAK2/STAT3 axis and improve the outcome of spinal cord injury. J Neuroinflamm. 2023;20(1).
31. Zhao YH, Peng F, He JY, Qu YL, Ni HM, Wu LL, et al. SOCS1 Peptidomimetic Alleviates Glomerular Inflammation in MsPGN by Inhibiting Macrophage M1 Polarization (vol 46, pg 2402, 2023). Inflammation. 2023;46(6).
32. Bidgood GM, Keating N, Doggett K, Nicholson SE. SOCS1 is a critical checkpoint in immune homeostasis, inflammation and tumor immunity. Front Immunol. 2024;15.
33. Li JY, Zhou HF, Fu XX, Zhang M, Sun F, Fan H. Dynamic role of macrophage CX3CR1 expression in inflammatory bowel disease. Immunol Lett. 2021;232:39-44.
34. Ziogas A, Bruno M, van der Meel R, Mulder WJM, Netea MG. Trained immunity: Target for prophylaxis and therapy. Cell Host Microbe. 2023;31(11):1776-91.

647 35. Ochando J, Mulder WJM, Madsen JC, Netea MG, Duivenvoorden R. Trained immunity - basic
648 concepts and contributions to immunopathology. Nat Rev Nephrol. 2023;19(1):23-37.
649 36. Sauceda C, Bayne C, Sudqi K, Gonzalez A, Dulai PS, Knight R, et al. Stool multi-omics for the
650 study of host-microbe interactions in inflammatory bowel disease. Gut Microbes. 2022;14(1).
651 37. Schaubeck M, Clavel T, Calasan J, Lagkouvardos I, Haange SB, Jehmlich N, et al. Dysbiotic gut
652 microbiota causes transmissible Crohn's disease-like ileitis independent of failure in antimicrobial
653 defence. Gut. 2016;65(2):225-37.
654 38. Palmela C, Chevarin C, Xu ZL, Torres J, Sevrin G, Hirten R, et al. Adherent-invasive *Escherichia*
655 *coli* in inflammatory bowel disease. Gut. 2018;67(3):574-87.
656 39. Kirchgesner J, Lemaitre M, Carrat F, Zureik M, Carbonnel F, Dray-Spira R. Risk of Serious and
657 Opportunistic Infections Associated With Treatment of Inflammatory Bowel Diseases.
658 Gastroenterology. 2018;155(2):337-+.
659 40. Hu ZD, Lu SH, Lowrie DB, Fan XY. Trained immunity: A Yin-Yang balance. Medcomm.
660 2022;3(1).
661 41. Ospelt C, Reedquist KA, Gay S, Tak PP. Inflammatory memories: Is epigenetics the missing link
662 to persistent stromal cell activation in rheumatoid arthritis? Autoimmun Rev. 2011;10(9):519-24.
663 42. Grigoriou M, Banos A, Filia A, Pavlidis P, Giannouli S, Karali V, et al. Transcriptome
664 reprogramming and myeloid skewing in haematopoietic stem and progenitor cells in systemic lupus
665 erythematosus. Ann Rheum Dis. 2020;79(2):242-53.
666 43. Tercan H, Riksen NP, Joosten LAB, Netea MG, Bekkering S. Trained Immunity: Long-Term
667 Adaptation in Innate Immune Responses. Arterioscl Throm Vas. 2021;41(1):55-61.
668 44. Liu S, Cao YQ, Cui KR, Ren G, Zhao TT, Wang XZ, et al. Regulation of T helper cell
669 differentiation by the interplay between histone modification and chromatin interaction. Immunity.
670 2024;57(5).
671 45. Kosinsky RL, Gonzalez MM, Saul D, Barros LL, Sagstetter MR, Fedyshyn Y, et al. The FOXP3^{+}
672 Pro-Inflammatory T Cell: A Potential Therapeutic Target in Crohn's Disease. Gastroenterology.
673 2024;166(4).
674 46. Britton GJ, Contijoch EJ, Mogno I, Vennaro OH, Llewellyn SR, Ng R, et al. Microbiotas from
675 Humans with Inflammatory Bowel Disease Alter the Balance of Gut Th17 and RORγt+ Regulatory T
676 Cells and Exacerbate Colitis in Mice. Immunity. 2019;50(1):212-+.
677 47. Almeida FF, Belz GT. Innate lymphoid cells: models of plasticity for immune homeostasis and
678 rapid responsiveness in protection. Mucosal Immunol. 2016;9(5):1103-12.
679 48. Hernández-Chirlaque C, Aranda CJ, Ocón B, Capitán-Cañadas F, Ortega-González M, Carrero JJ,
680 et al. Germ-free and Antibiotic-treated Mice are Highly Susceptible to Epithelial Injury in DSS Colitis.
681 J Crohns Colitis. 2016;10(11):1324-35.
682 49. Panpetch W, Hiengrach P, Nilgate S, Tumwasorn S, Somboonna N, Wilantho A, et al. Additional
683 *Candida albicans* administration enhances the severity of dextran sulfate solution induced colitis
684 mouse model through leaky gut-enhanced systemic inflammation and gut-dysbiosis but attenuated by
685 *Lactobacillus rhamnosus* L34. Gut Microbes. 2020;11(3):465-80.
686 50. Rupper AC, Cardelli JA. Induction of guanylate binding protein 5 by gamma interferon increases
687 susceptibility to Salmonella enterica serovar Typhimurium-induced pyroptosis in RAW 264.7 cells.
688 Infect Immun. 2008;76(6):2304-15.

51. Rigamonti A, Villar J, Segura E. Monocyte differentiation within tissues: a renewed outlook. Trends Immunol. 2023;44(12):999-1013.
52. Wynn TA, Vannella KM. Macrophages in Tissue Repair, Regeneration, and Fibrosis. Immunity. 2016;44(3):450-62.
53. De Schepper S, Verheijden S, Aguilera-Lizarraga J, Viola MF, Boesmans W, Stakenborg N, et al. Self-Maintaining Gut Macrophages Are Essential for Intestinal Homeostasis (vol 175, pg 400, 2018). Cell. 2019;176(3):676-.
54. Bain CC, Scott CL, Uronen-Hansson H, Gudjonsson S, Jansson O, Grip O, et al. Resident and pro-inflammatory macrophages in the colon represent alternative context-dependent fates of the same Ly6Chi monocyte precursors. Mucosal Immunol. 2013;6(3):498-510.
55. Trebicka E, Shanmugam NKN, Chen KJ, Su CW, Shi HN, Cherayil BJ. Intestinal Inflammation Leads to a Long-lasting Increase in Resistance to Systemic Salmonellosis that Requires Macrophages But Not B or T Lymphocytes at the Time of Pathogen Challenge. Inflamm Bowel Dis. 2015;21(12):2758-65.
56. Weber B, Saurer L, Schenk M, Dickgreber N, Mueller C. CX3CR1 defines functionally distinct intestinal mononuclear phagocyte subsets which maintain their respective functions during homeostatic and inflammatory conditions. Eur J Immunol. 2011;41(3):773-9.
57. Zhang B, Moorlag SJ, Dominguez-Andres J, Bulut O, Kilic G, Liu Z, et al. Single-cell RNA sequencing reveals induction of distinct trained-immunity programs in human monocytes. J Clin Invest. 2022;132(7).
58. Leonhardt J, Grosse S, Marx C, Siwczak F, Stengel S, Bruns T, et al. Candida albicans beta-Glucan Differentiates Human Monocytes Into a Specific Subset of Macrophages. Front Immunol. 2018;9:2818.
59. Camilli G, Bohm M, Piffer AC, Lavenir R, Williams DL, Neven B, et al. beta-Glucan-induced reprogramming of human macrophages inhibits NLRP3 inflammasome activation in cryopyrinopathies. J Clin Invest. 2020;130(9):4561-73.
60. Hajishengallis G, Li X, Mitroulis I, Chavakis T. Trained Innate Immunity and Its Implications for Mucosal Immunity and Inflammation. Adv Exp Med Biol. 2019;1197:11-26.
61. Yui SR, Nakamura T, Sato T, Nemoto Y, Mizutani T, Zheng X, et al. Functional engraftment of colon epithelium expanded in vitro from a single adult $Lgr5^{+}$ stem cell. Nat Med. 2012;18(4):618-23.
62. Lopetuso LR, Deleu S, Godny L, Petito V, Puca P, Facciotti F, et al. The first international Rome consensus conference on gut microbiota and faecal microbiota transplantation in inflammatory bowel disease. Gut. 2023;72(9):1642-50.
63. Haifer C, Luu LDW, Paramsothy S, Borody TJ, Leong RW, Kaakoush NO. Microbial determinants of effective donors in faecal microbiota transplantation for UC. Gut. 2023;72(1):90-100.

729 **Fig 1. β-glucan (BG) pretreatment ameliorates DSS-induced colitis.**

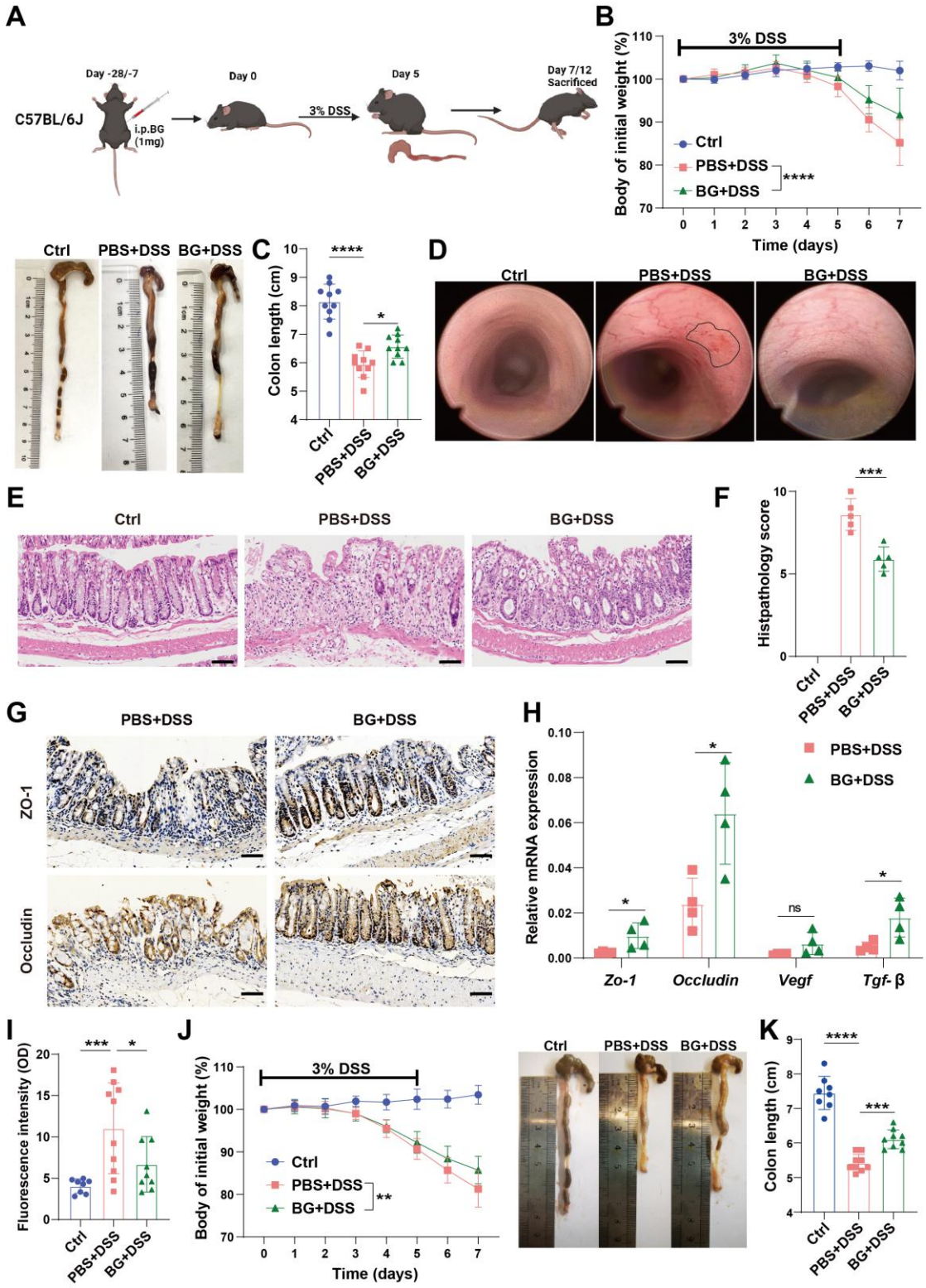

730

731 **(**A) Schematic representation of BG-induced trained immunity and DSS colitis model, (**B**) Body
732 weight change curve of mice pretreated with BG for one week, followed by colitis induction with
733 3% DSS (n = 10), (**C**) Colon length changes in mice from (**B**), (**D**) Endoscopic images displaying
734 mucosal damage, (**E and F**) H&E staining and histological scoring. Scale bars: 100 μm, (**G and H)**
735 Expression levels of tight junction and repair, (**I**) FITC-dextran assay assessing intestinal barrier
736 function, (**J**) Body weight change curve of mice pretreated with BG for four weeks, followed by
737 colitis induction with 3% DSS (n = 8-9), (**K**) Colon length changes in mice from (**J**). Data are
738 presented as mean ± SD. Statistical significance: *$p < 0.05$, **$p < 0.01$, ***$p < 0.001$, ****$p <$
739 0.0001. ns, not significant.

740

741

742

743

744

745

746

747

748

749

750

751

752

753

Fig 2. BG ameliorates colitis by enhancing myeloid cell activation.

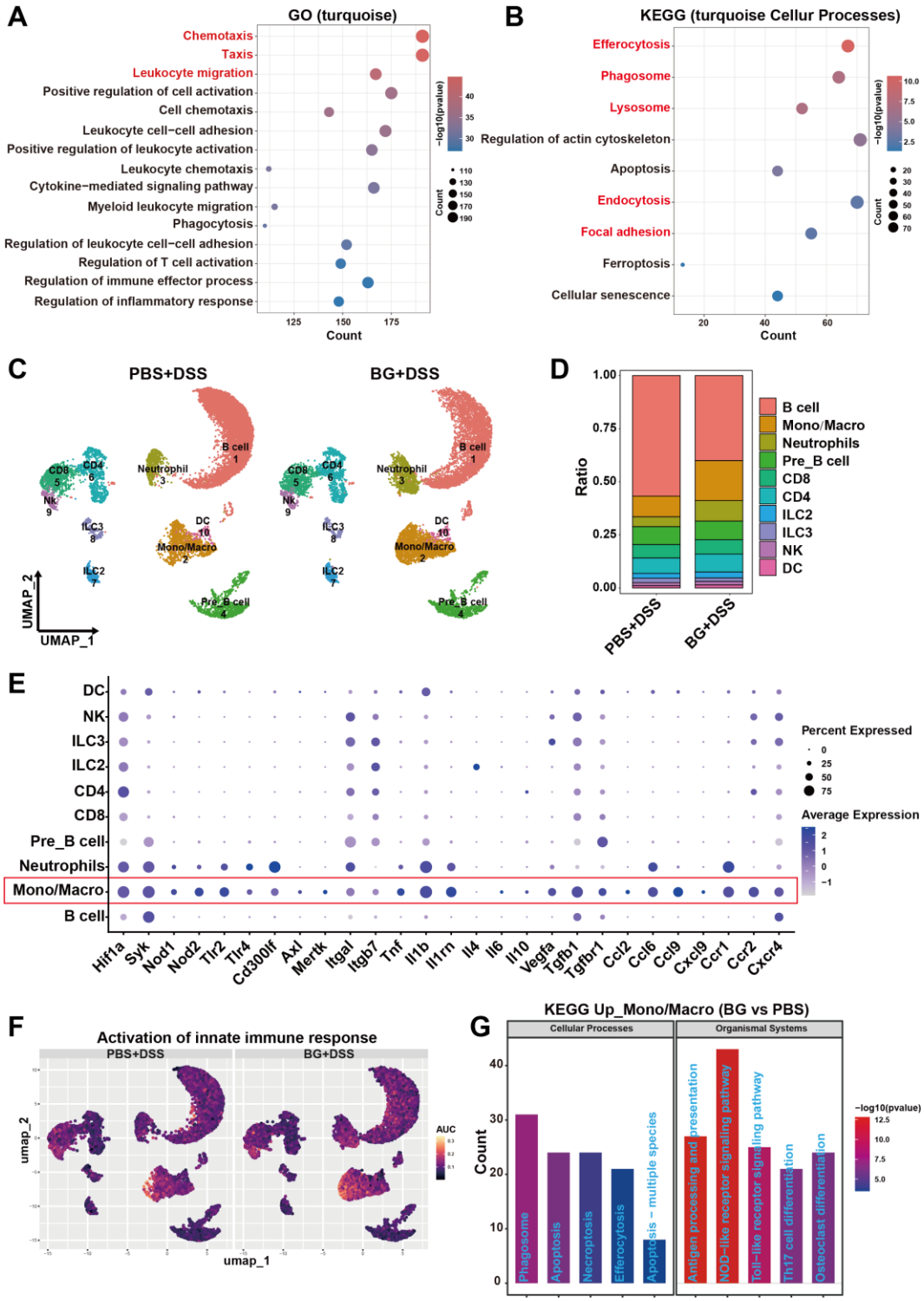

757 RNA sequencing of colon tissue at different time points of colitis. (**A**) GOBP and (**B**) KEGG
758 pathway analyses of genes in the MEturquoise module. Single-cell RNA sequencing analysis of
759 $CD45^+$ cells in the colon on day seven of colitis after one week of BG pretreatment. (**C**) UMAP
760 plot of LP $CD45^+$ cells, (**D**) Cell ratio distribution from scRNA-seq data, (**E**) Dot plots showing
761 representative DEGs between LP $CD45^+$ cells, (**F**) AUC scores for selected pathways, (**G**) KEGG
762 pathway analysis of genes upregulated in the monocyte-macrophage lineage. DEGs, differentially
763 expressed genes. LP, lamina propria. UMAP, uniform manifold approximation, and projection.
764 AUC, area under the curve.

765

766

767

768

769

770

771

772

773

774

775

776

777

778

779

780 **Fig 3. BG trained bone marrow monocytes protected against colitis via the**
781 **Ccl2-Ccr2 axis.**

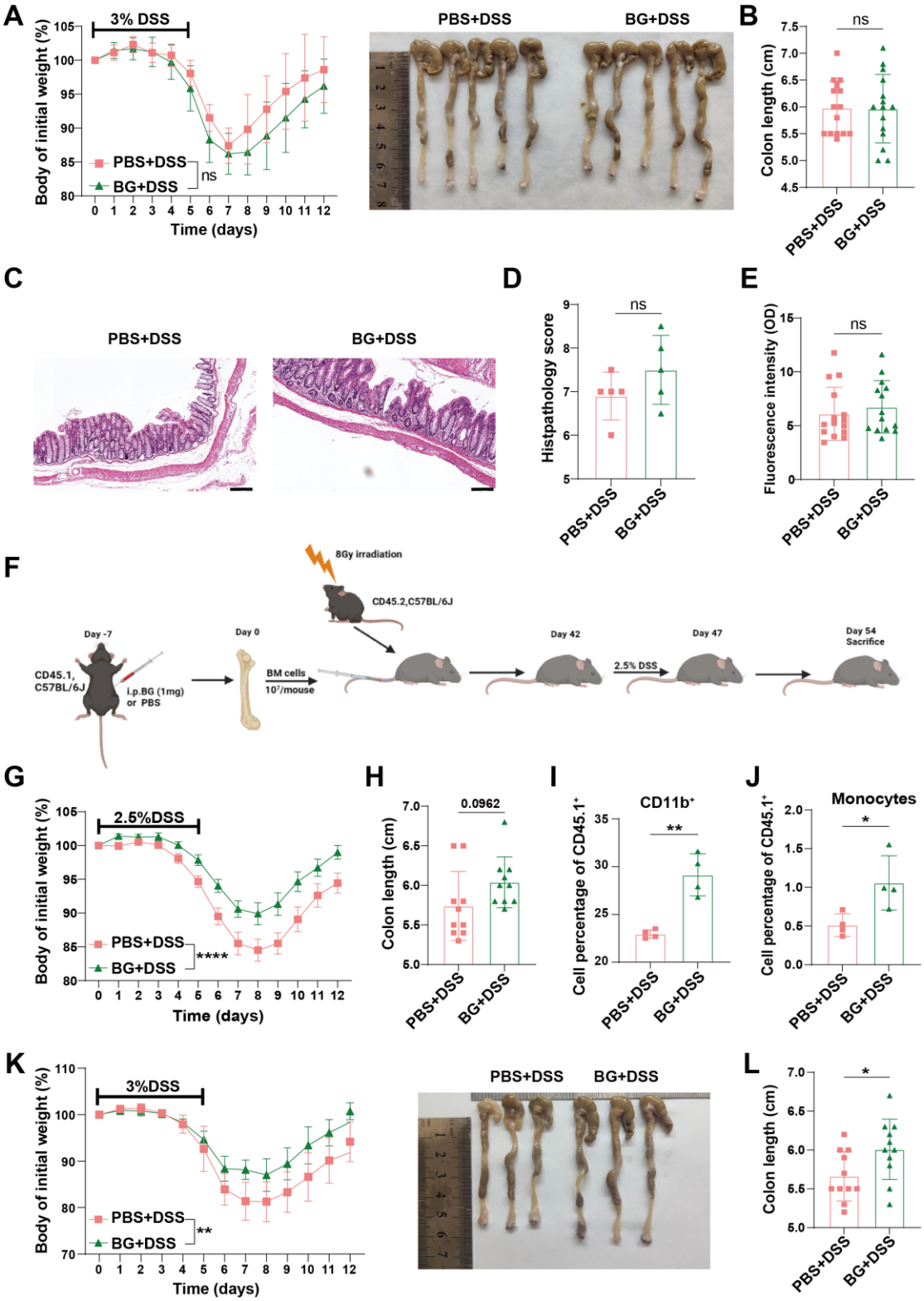

782

783 *Ccr2*$^{-/-}$ mice pretreated with BG for 1 week followed by induction of colitis with 3% DSS. (**A**)
784 Changes in body weight (n = 15), (**B**) Colon length changes in *Ccr2*$^{-/-}$ mice from (**A**), (**C and D**)
785 H&E staining and histological scoring, H&E. Scale bars: 100 μm, (**E**) FITC-dextran assay
786 assessing intestinal barrier function, (**F**) Schematic representation of bone marrow transplantation
787 from BG-pretreated CD45.1 mice to CD45.2 mice and colitis model, (**G**) Body weight change
788 curve of colitis mice (n = 10), (**H**) Colon length changes in colitis mice from (**G**), (**I and**
789 **J**)Percentage of CD11b^{+} (**I**) and Ly6C^{hi} monocytes (**J**) were analyzed by flow cytometry in
790 peripheral blood, (**K and L**) Body weight change curve(**K**) and colon length changes of *Ccr2*$^{-/-}$
791 mice receiving Ly6C^{hi} monocyte adoptive transfer(**L**) (n = 11). Data are presented as mean ± SD.
792 Statistical significance: *p <0.05, **p <0.01, ****p <0.0001. ns, not significant.

793

794

795

796

797

798

799

800

801

802

803

804

805

806

Fig 4. BG-trained monocytes enhance innate immune activation and microbial control.

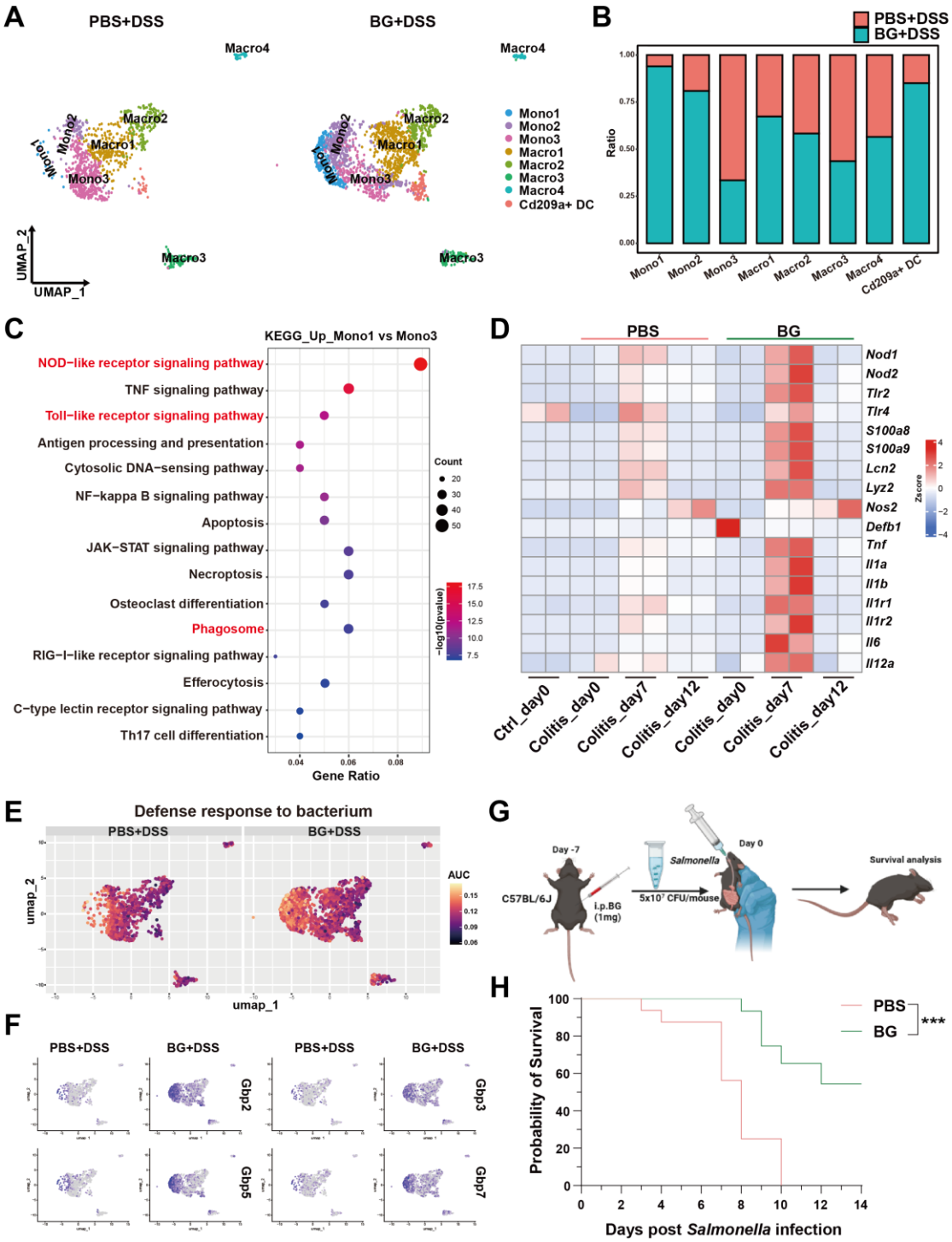

812 (**A**) UMAP and graphical visualization of the monocyte/macrophage lineage, (**B**) The ratio of
813 monocyte/macrophage subsets, (**C**) KEGG pathway enrichment analysis of genes upregulated in
814 monocyte 1 and monocyte 3, (**D**) Gene expression analysis at different time points of colitis, based
815 on colon RNA sequencing, (**E**) AUC scores of selected pathways, (**F**) UMAP plots showing
816 differential gene expression patterns, (**G**) Schematic representation *Salmonella* resistance after one
817 week of BG pretreatment, (**H**) Survival curve of mice infected with *Salmonella* after one week of
818 BG training. Statistical significance: ***$p < 0.001$.

819

820

821

822

823

824

825

826

827

828

829

830

831

832

833

Fig 5. BG-mediated reprogramming of myeloid differentiation trajectories balances inflammation and enhances mucosal repair in colitis.

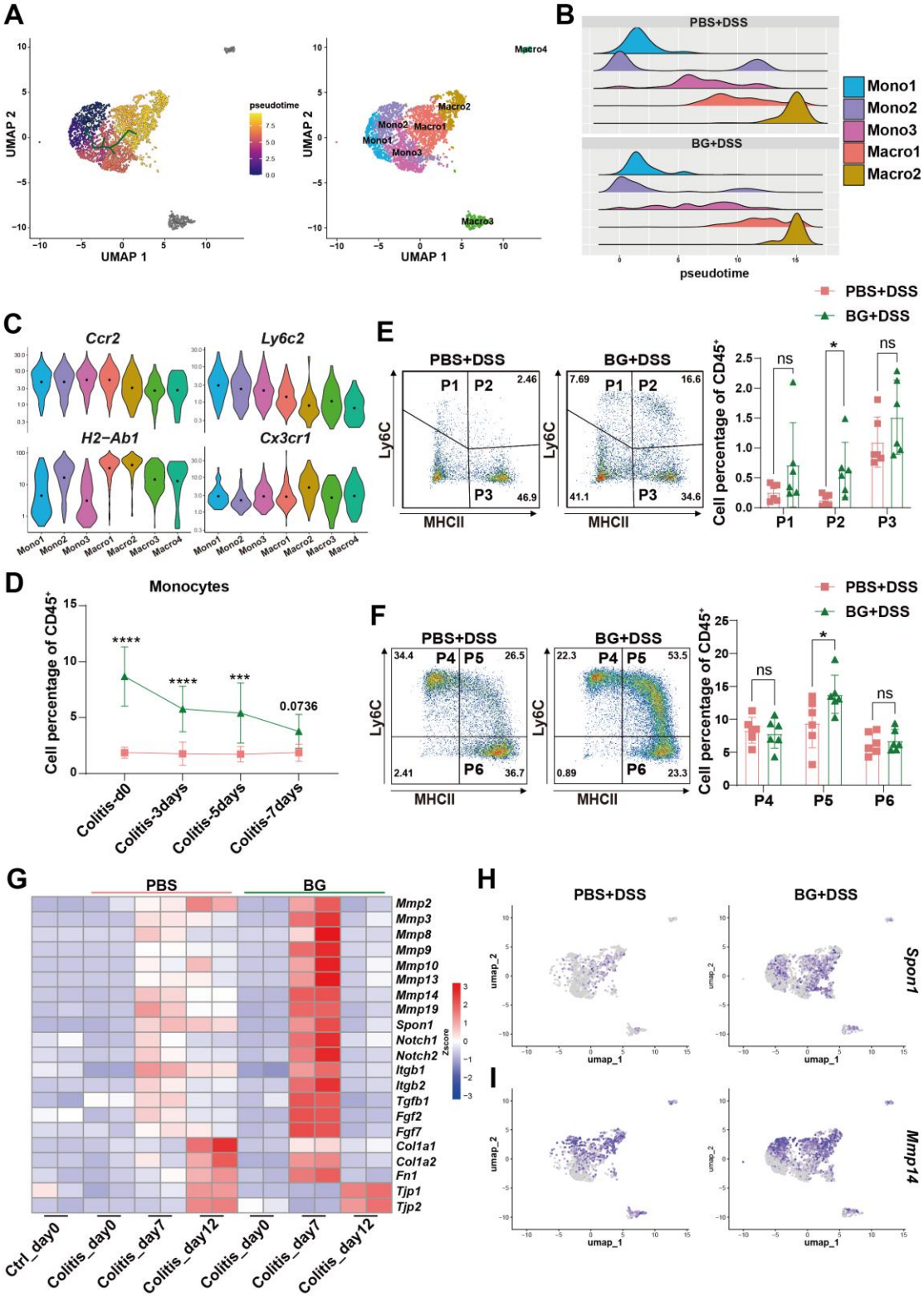

(**A**) Monocle 3 trajectory analysis of monocyte/macrophage subsets, (**B**) Ridgeline plot of monocyte/macrophage subsets, (**C**) Violin plots of surface marker gene expression in monocyte/macrophage subsets, (**D**) Percentage of monocytes in peripheral blood at different time points of colitis progression, (**E and F**) Colonic LPMCs were collected, and the percentages of monocyte/macrophage were analyzed on day 7 of colitis, (**G**) Expression of mucosal repair-related genes at different time points of colitis, (**H**) Gene expression analysis of the monocyte/macrophage lineage. Data are presented as mean ± SD. Statistical significance: *p <0.05, ***p <0.001; ****p <0.0001. ns, not significant.

Graphical abstract

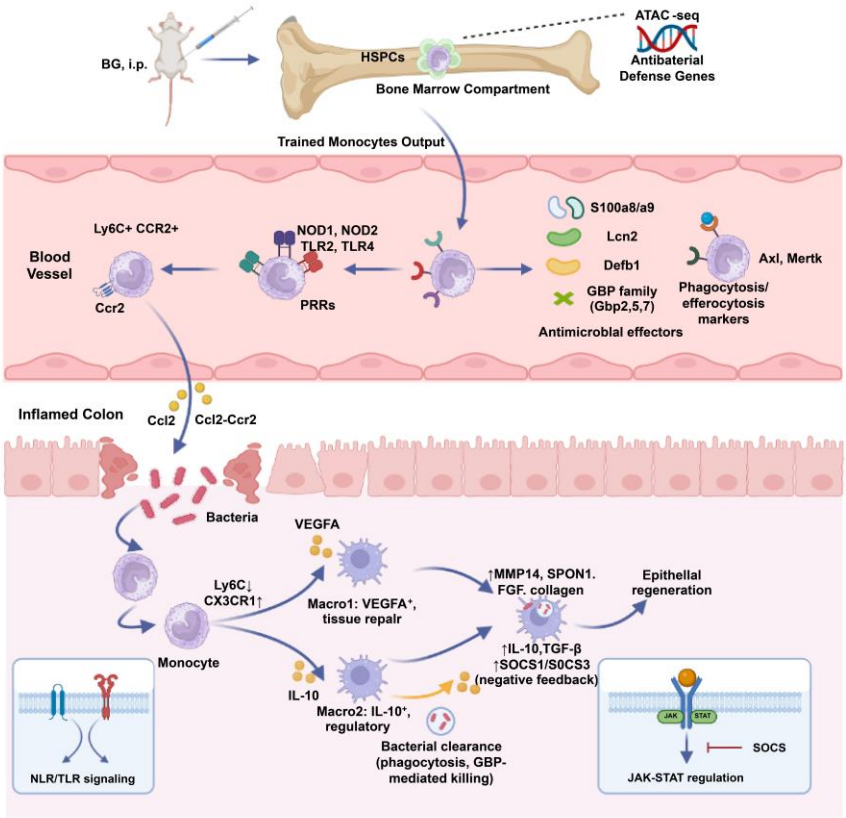

850 **Fig S1. BG pretreatment ameliorates DSS-induced colitis.**

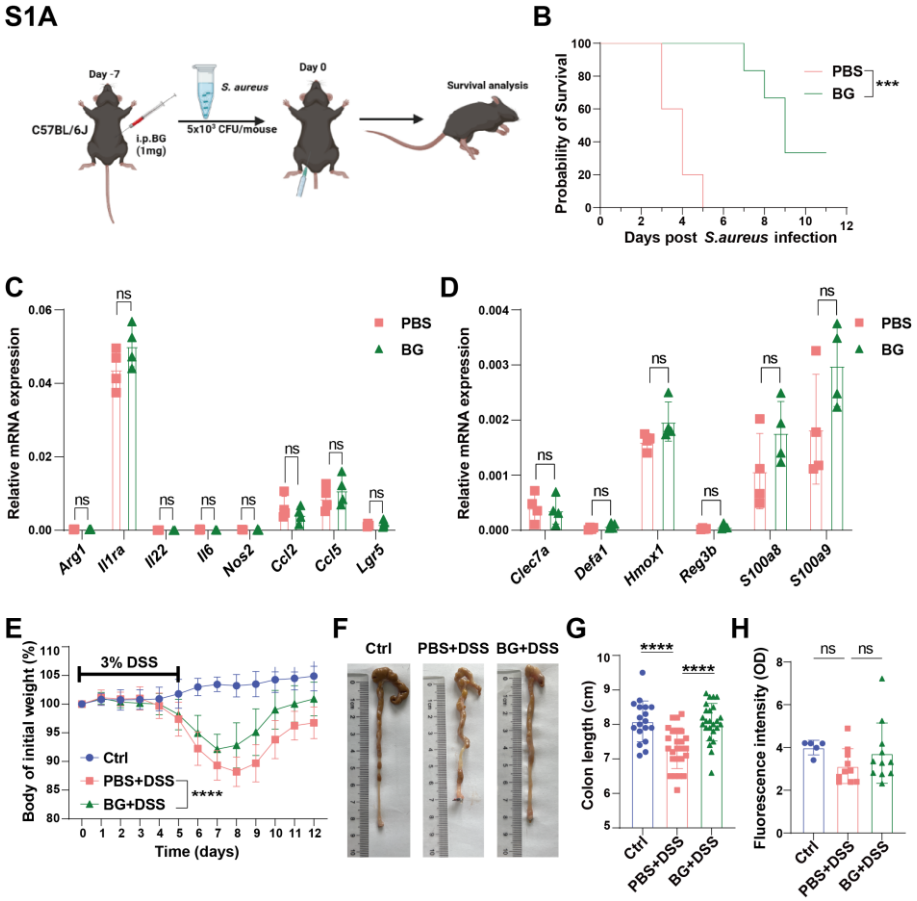

851

852 (**A**) Schematic representation of BG-induced trained immunity and *Staphylococcus aureus*
853 infection model, (**B**) Survival curve of mice infected with *Staphylococcus aureus,* (**C and D**) The
854 gene expression of inflammatory mediators and antibacterial were analyzed by qRT-PCR, (**E**)
855 Body weight change curve of mice pretreated with BG for one week, followed by colitis induction
856 with 3% DSS (n = 18-25), (**F and G**) Changes of colon length from (**E**), (**H**) FITC-dextran assay
857 assessing intestinal barrier function (n = 5-11). Data are presented as mean ± SD. Statistical
858 significance: *$p < 0.05$, ***$p < 0.001$; ****$p < 0.0001$. ns, not significant.

859

860

861

862

863

864

865 **Fig S2. BG pretreatment 4 or 7 weeks ameliorates DSS-induced colitis.**

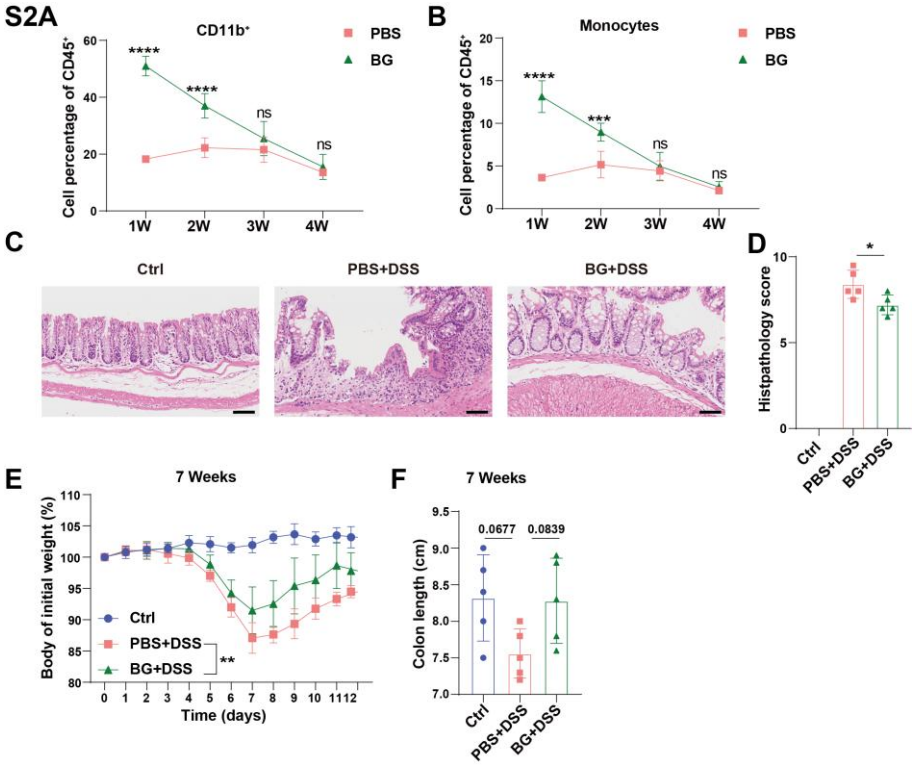

866

867 (**A and B**) Percentage of myeloid cells and monocytes in the peripheral blood of mice at different
868 time points after one week of BG pretreatment, (**C and D**) H&E staining, and histological scoring
869 of colitis mice after four weeks of BG training. Scale bars: 100 μm, (**E**) Body weight change curve
870 of mice pretreated with BG for seven weeks, followed by colitis induction with 3% DSS, (**F**)
871 Changes of colon length from (**E**) (n = 5). Data are presented as mean ± SD. Statistical
872 significance: *$p < 0.05$, **$p < 0.01$, ***$p < 0.001$, ****$p < 0.0001$. ns, not significant.

873

874

875

876

877

878

879 **Fig S3. BG pretreatment ameliorates colitis is independent of adaptive immunity.**

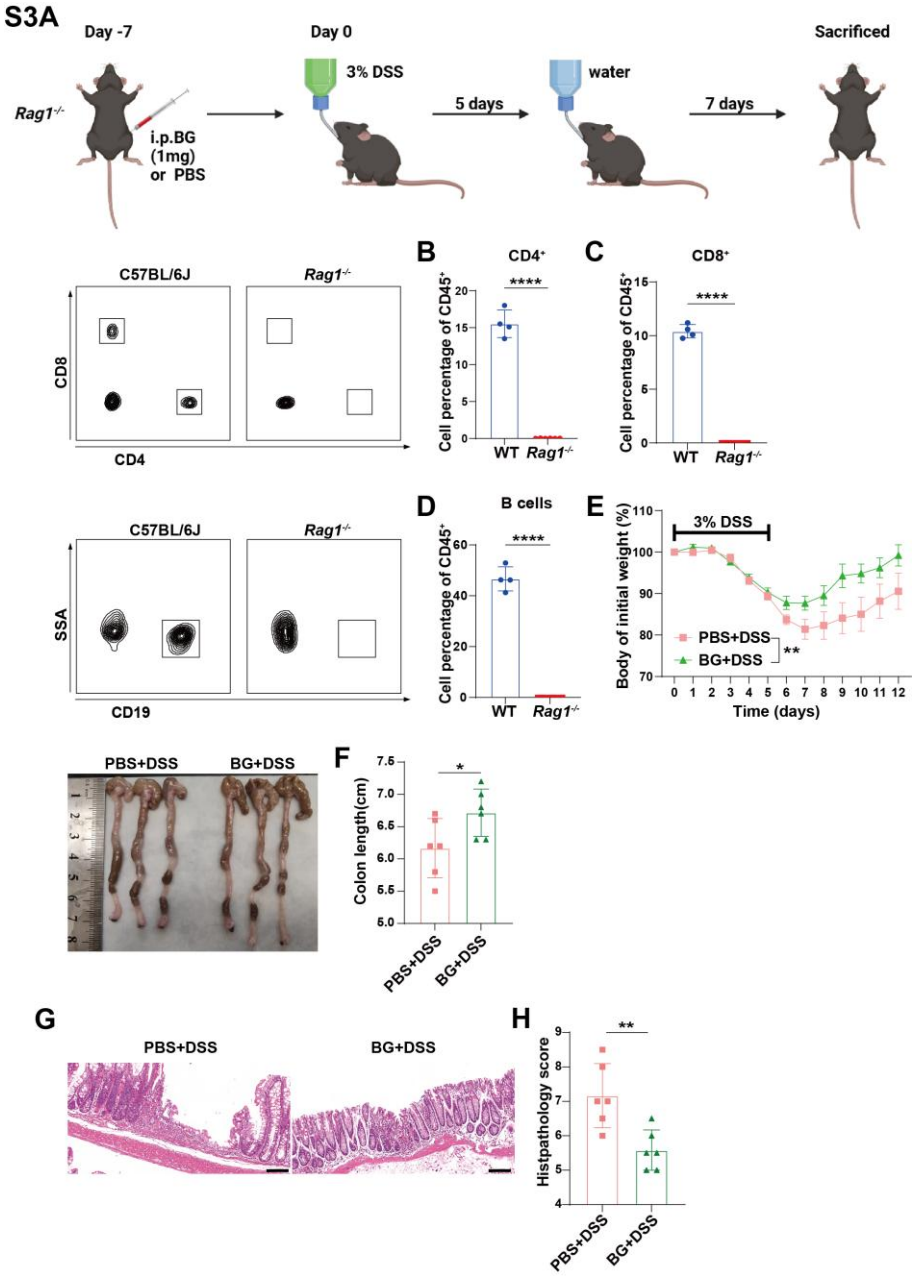

880

881 (**A**) Schematic representation of BG-induced trained immunity and DSS colitis model in *Rag1*$^{-/-}$
882 mice, (**B-D**) Flow cytometry analysis of peripheral blood from *Rag1*$^{-/-}$ mice, (**E**) Body weight
883 change curve of *Rag1*$^{-/-}$ mice pretreated with BG for one week, followed by colitis induction with
884 3% DSS, (**F**) Colon length changes in *Rag1*$^{-/-}$ mice from (**E**), (**G and H**) H&E staining and
885 histological scoring. Scale bars: 100 μm. Data are presented as mean ± SD. Statistical significance:
886 $*p < 0.05$, $**p < 0.01$, $****p < 0.0001$.

887 **Fig S4. BG ameliorates colitis by enhancing myeloid cell activation.**

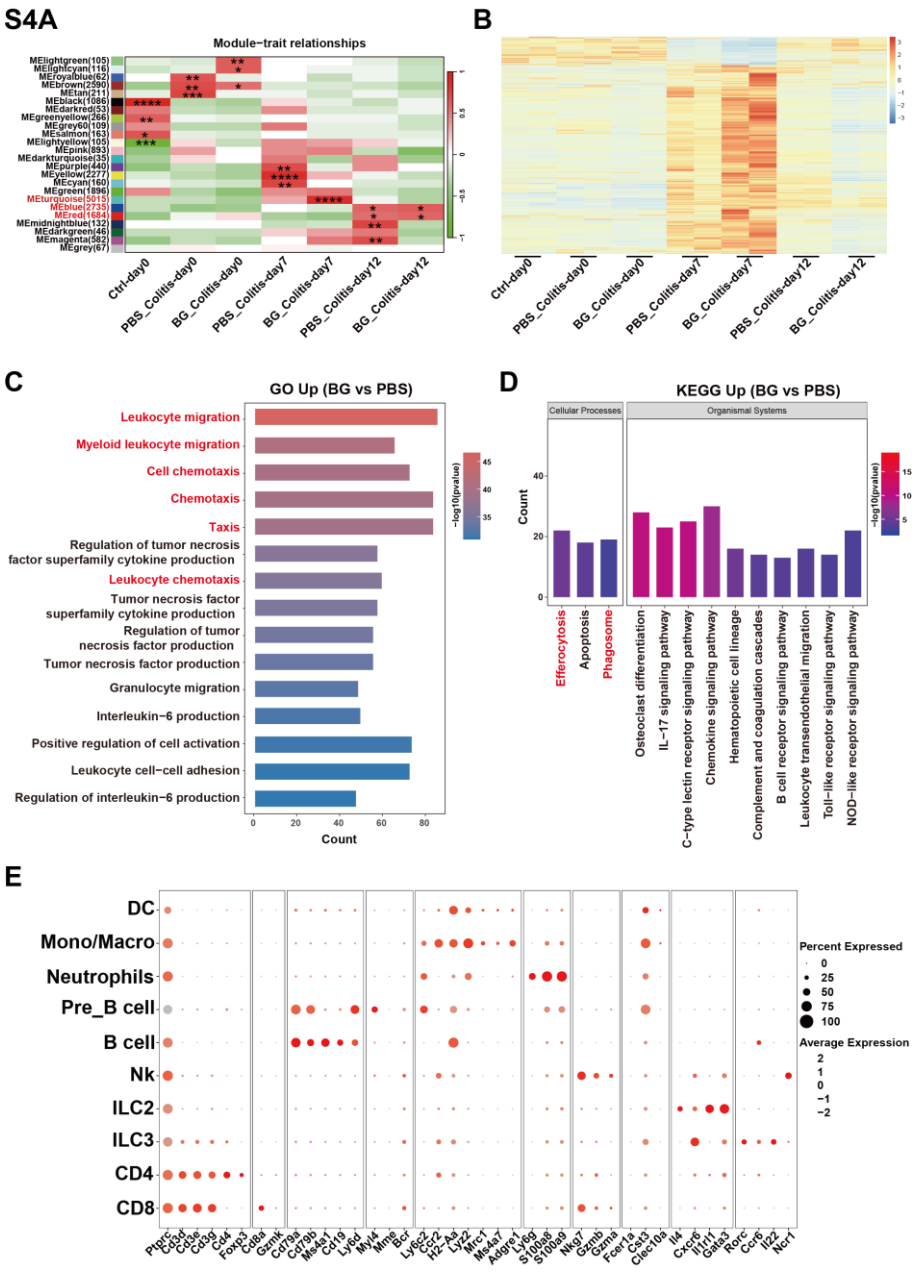

888

889 (**A**) RNA sequencing of colon tissue at different time points during colitis, with WGCNA
890 identifying major gene modules, (**B**) DEGs in the Meturquoise module, (**C and D**) GO and KEGG
891 pathway analysis of colon tissue on day seven of colitis after one week of BG pretreatment, (**E**)
892 Expression of marker genes in LP CD45^{+} cells on day seven of colitis after one week of BG
893 pretreatment.

894 **Fig S5. BG trained bone marrow monocytes protected against colitis via the**
895 **Ccl2-Ccr2 axis.**

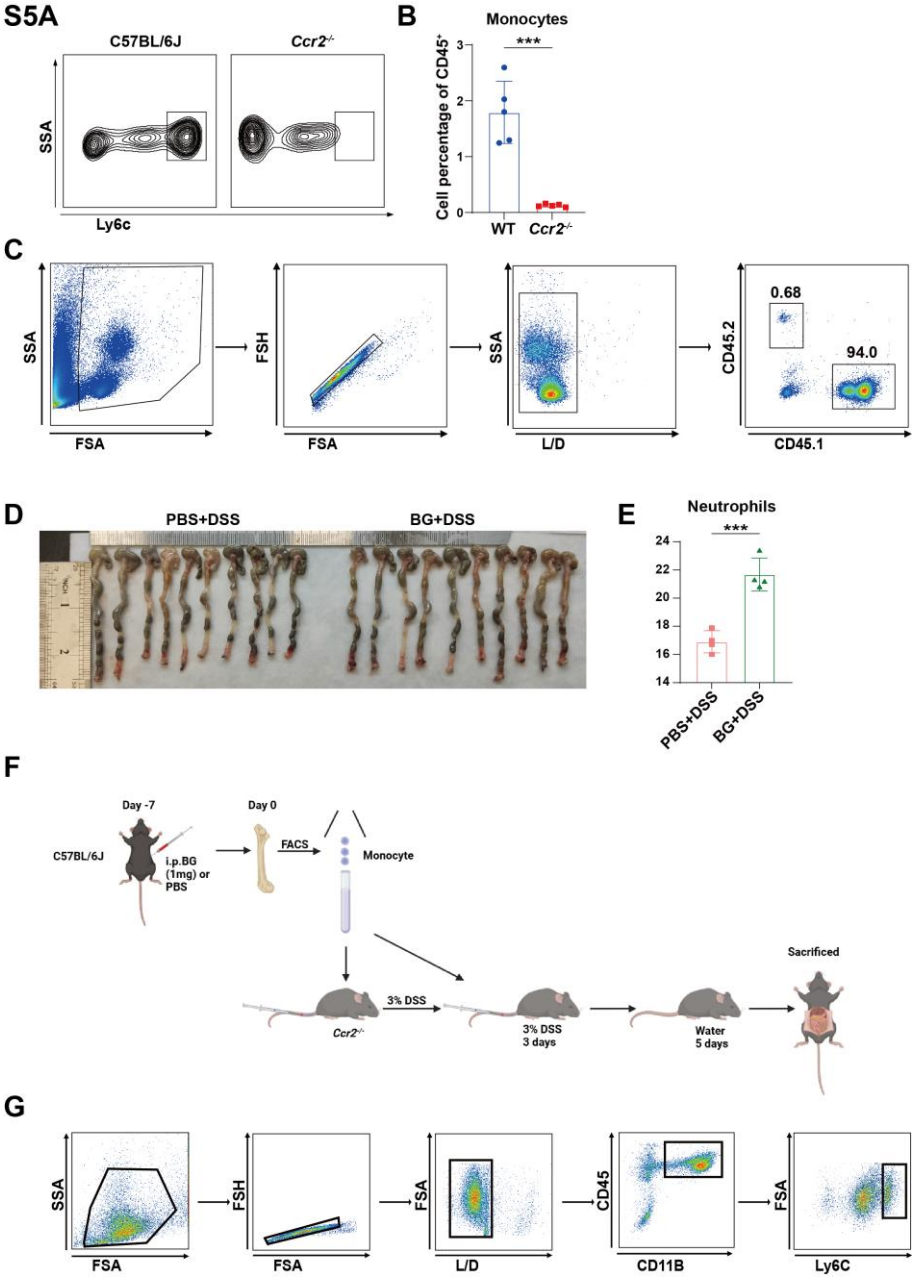

896

897 (**A and B**) Flow cytometry analysis of peripheral blood from *Ccr2*$^{-/-}$ mice, (**C**) Flow cytometry
898 analysis of bone marrow reconstitution in CD45.2 recipient mice, (**D**) Colon length changes in
899 bone marrow transplantation experiments from BG-pretreated CD45.1 mice to CD45.2 mice, (**E**)
900 Percentage of Ly6G^{+} neutrophils in peripheral blood of CD45.2 recipient mice, (**F**) Bone marrow

monocytes transplant model, (**G**) Flow sorting scheme of bone marrow monocytes. Data are presented as mean ± SD. Statistical significance: ***$p < 0.001$.

Fig S6. BG pretreatment enhances innate immunity and phagocytic capacity.

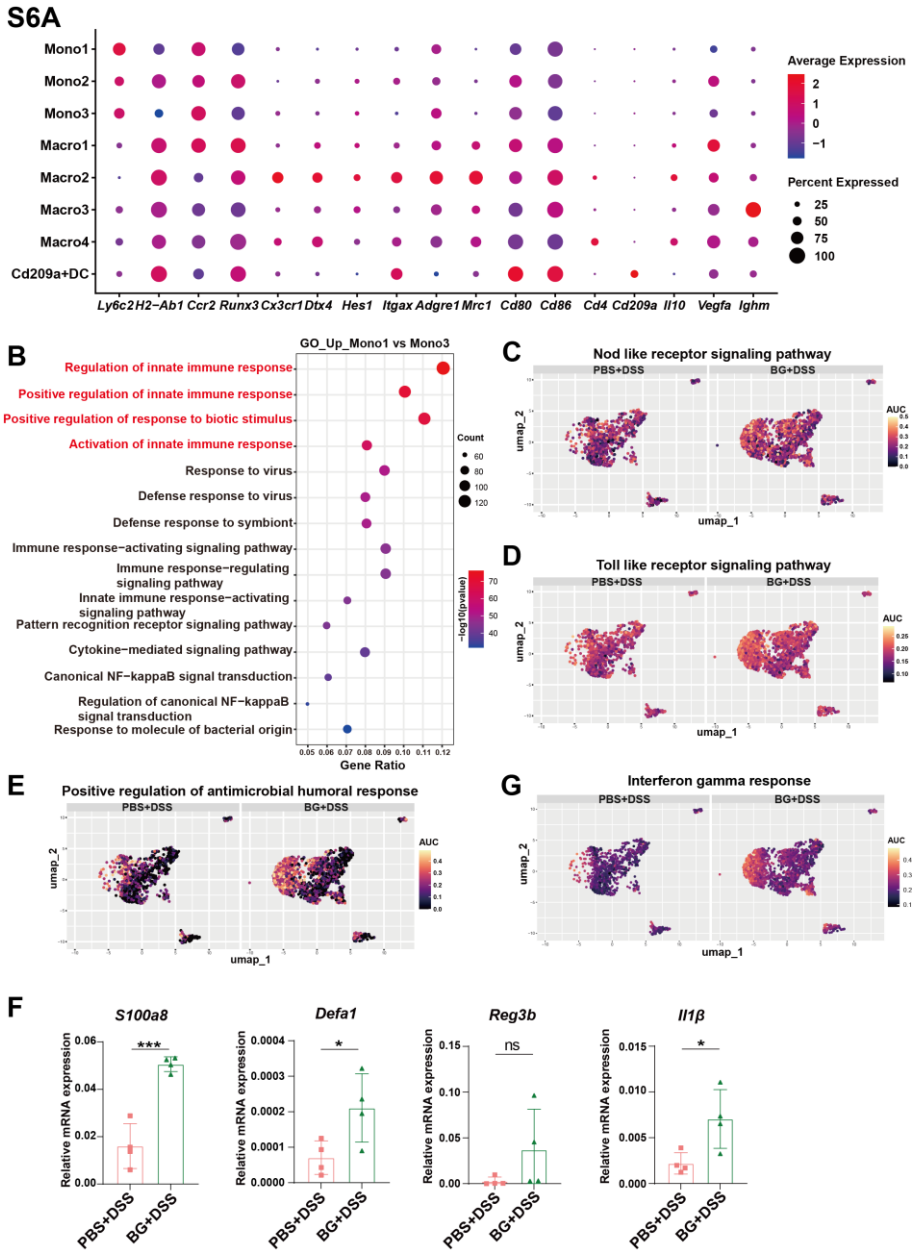

(**A**) Major marker genes of eight cell clusters within the monocyte/macrophage lineage, (**B**) GO analysis of genes upregulated in monocytes 1 and monocyte 3, (**C-E**) AUC scores of selected pathways, (**F**) Antibacterial gene expression was analyzed by qRT-PCR. (**G**) AUC scores of

selected pathways. Data are presented as mean ± SD. Statistical significance: *$p < 0.05$, ***$p < 0.001$, ns, not significant.

Figure S7. BG induced immune-related epigenomic remodeling in monocytes.

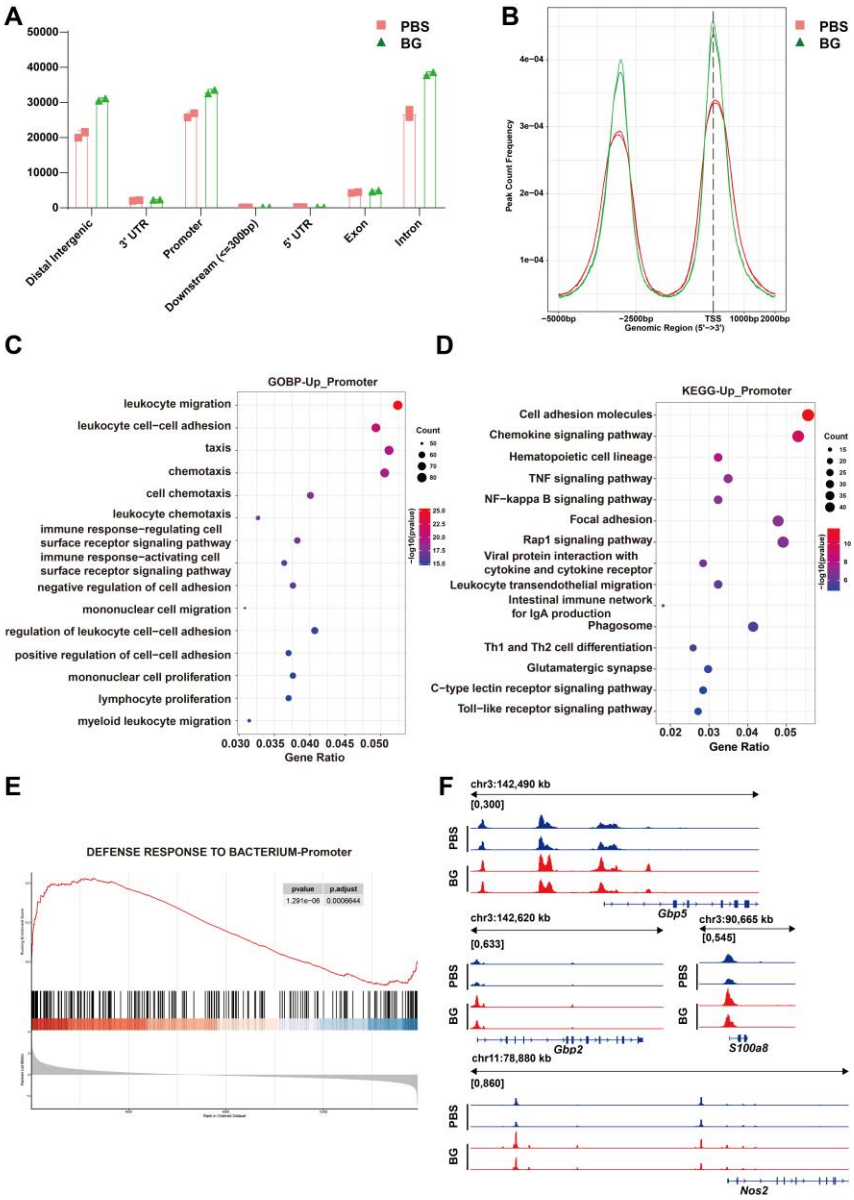

This figure delineates β-glucan (BG)-mediated epigenomic reprogramming in PBS (control) vs. BG-treated monocytes.

(A) Bar plot of chromatin accessibility signal enrichment across genomic regions. Bars denote signal counts, showing BG-altered region-specific signal accumulation.

(B) Density plot of chromatin peaks relative to promoter TSS (±2000 bp). BG shifts peaks from TSS core to promoter flanks, indicating promoter-proximal epigenomic reorganization.

(C) GO BP bubble plot for genes with BG-upregulated promoter accessibility. Enriched terms focus on immune processes.

(D) KEGG pathway bubble plot enriched immune/inflammatory pathways support BG's role in trained immunity.

(E) Enrichment profile and heatmap for the "defense response to bacterium" promoter module, highlighting BG-induced epigenetic priming of antibacterial programs.

(F) Locus-specific chromatin accessibility tracks for selected immune genes, validating BG-induced epigenetic modifications in upstream regions relative to PBS controls.

Fig S8. BG-induced trained immunity promotes monocyte differentiation.

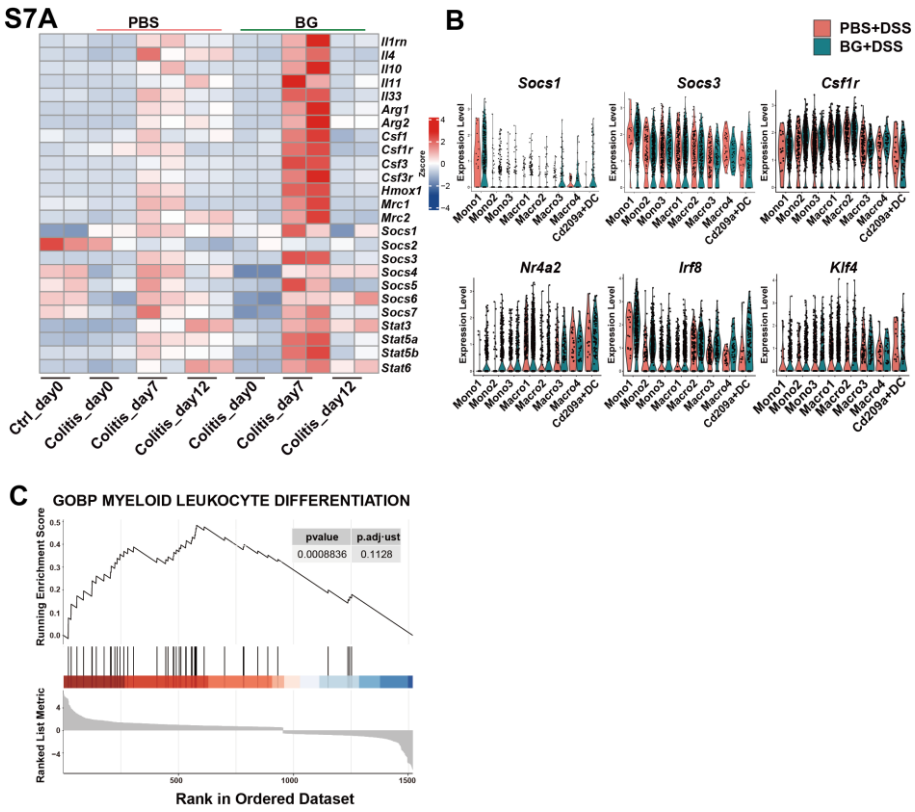

932 (**A**) Gene expression analysis at different time points of colitis, based on colon RNA sequencing,
933 (**B**) Violin plots of gene expression in eight cell clusters, (**C**) GSEA analysis showing gene
934 enrichment pattern on day seven of colitis.

935 **Fig S9 BG training downregulates the proportion of peripheral monocytes**
936 **during colitis development.**

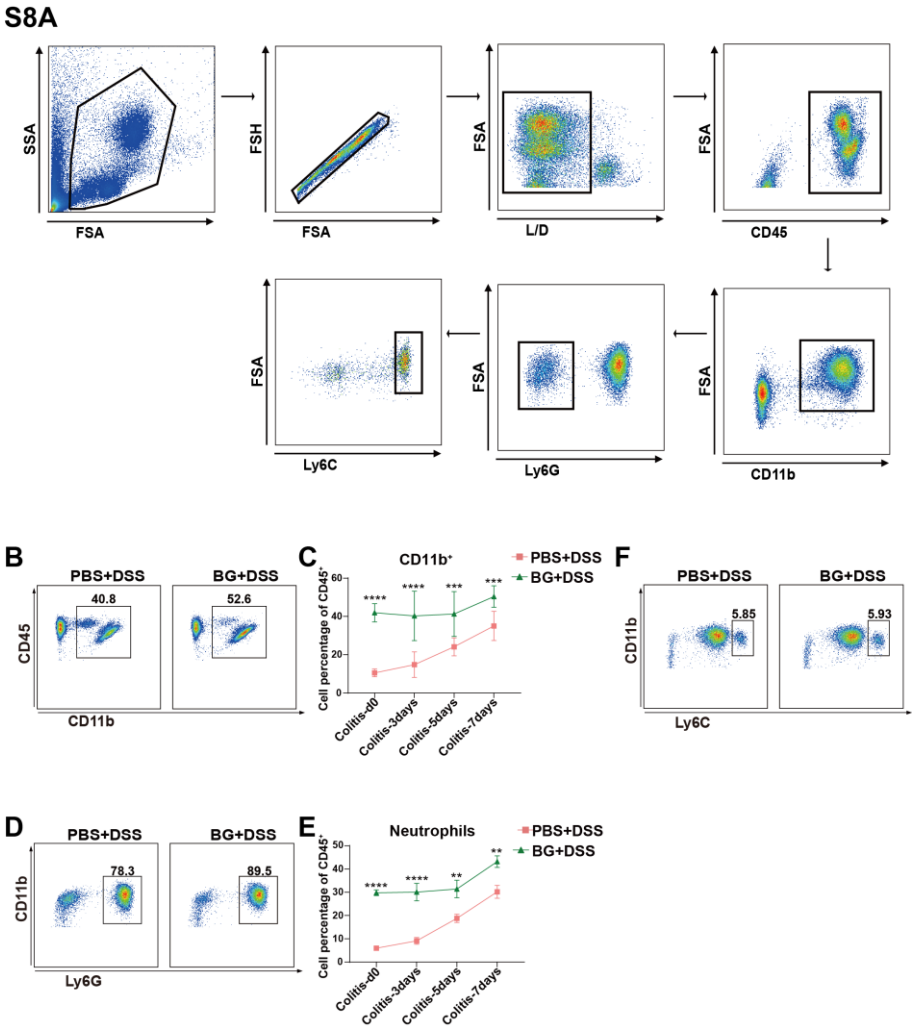

937

938 (**A**) Peripheral blood flow cytometry gating strategy, (**B**) Representative flow cytometry plots of
939 CD11b^{+} myeloid cells in peripheral blood on day seven of colitis (**C**) The percentage of CD11b^{+}
940 myeloid cells at different time points of colitis, (**D**) Representative flow cytometry plots of Ly6G^{+}
941 neutrophils in peripheral blood on day seven of colitis, (**E**) Percentage of Ly6G^{+} neutrophils at
942 different time points of colitis, (**F**) Representative flow cytometry plots of Ly6C^{hi} monocytes in

943 peripheral blood on day seven of colitis. Data are presented as mean ± SD. Statistical significance:

944 $^{**}p < 0.01$; $^{***}p < 0.001$; $^{****}p < 0.0001$.

945

946 **Fig S10 BG training upregulates the proportion of colonic**

947 **monocytes/macrophages in colitis mice.**

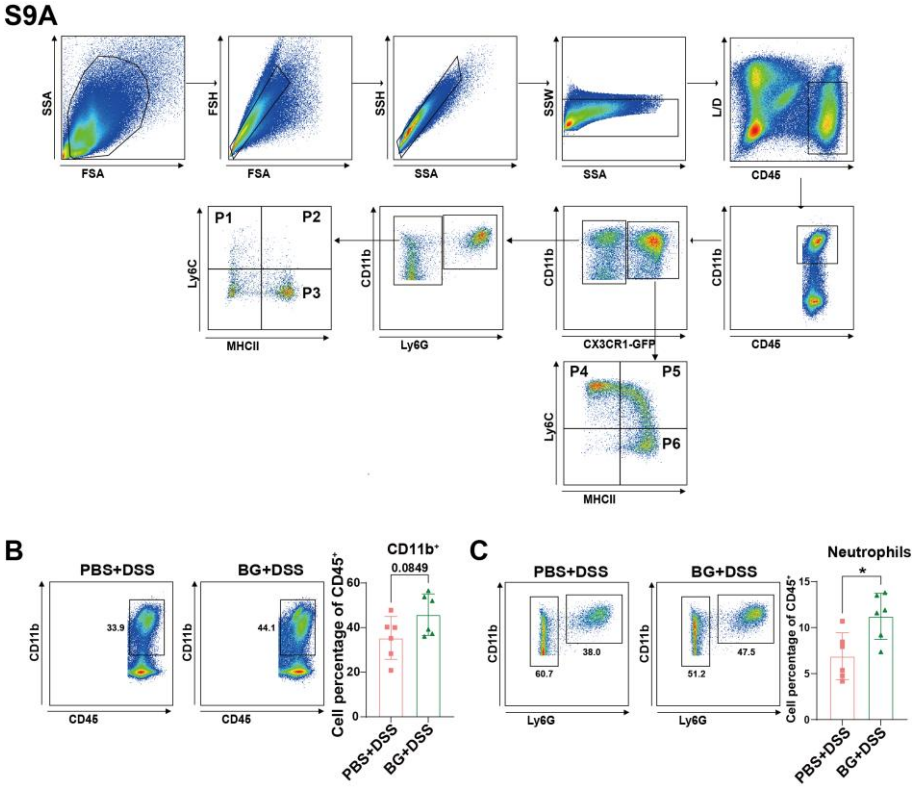

948

949 (**A**) Colonic LPMCs flow cytometry gating strategy, (**B and C**) The percentages of $CD11b^+$

950 myeloid cells (**B**) and $Ly6G^+$ neutrophils (**C**) were analyzed on day seven of colitis ($n = 6$). Data

951 are presented as mean ± SD. Statistical significance: $^{*}p < 0.05$. ns, not significant.

952

953

954

955

956

Fig S11 Adoptive transfer of BG-trained monocytes ameliorates experimental colitis.

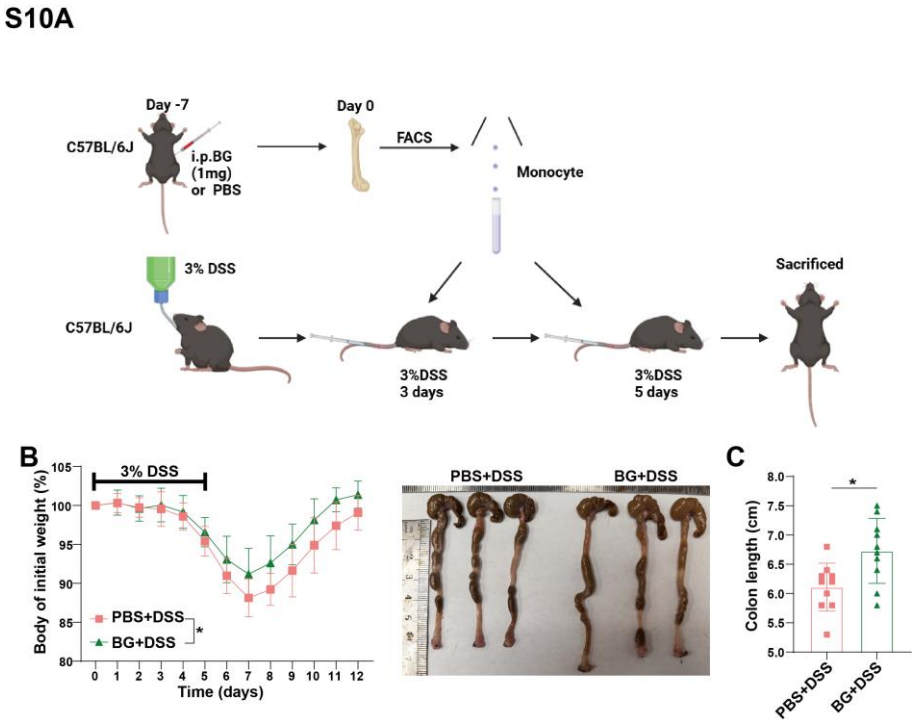

(**A**) Bone marrow monocytes transplant and colitis treatment model, (**B and C**) Body weight change curve (**B**) and colon length changes (**C**) in WT colitis mice receiving Ly6C^{hi} monocyte adoptive transfer (n = 10). Data are presented as mean ± SD. Statistical significance: *$p < 0.05$.